ELSEVIER

Nuclear Instruments and Methods in Physics Research A 432 (1999) 265–298

NUCLEAR INSTRUMENTS & METHODS IN PHYSICS RESEARCH Section A

www.elsevier.nl/locate/nima

The time-of-flight system for CLAS

E.S. Smith[a,*], T. Carstens[a], J. Distelbrink[b,1], M. Eckhause[c], H. Egiyan[c], L. Elouadrhiri[d], J. Ficenec[e], M. Guidal[f,2], A.D. Hancock[c,3], F.W. Hersman[b], M. Holtrop[b], D.A. Jenkins[e], W. Kim[g], K. Loukachine[e], K. MacArthur[b,4], C. Marchand[f], B. Mecking[a], G. Mutchler[h], D. Schutt[e], L.C. Smith[i], T.P. Smith[b,5], S. Taylor[h], T.Y. Tung[c,6], A. Weisenberger[a], R.E. Welsh[c]

[a]*Thomas Jefferson National Accelerator Facility, 12000 Jefferson Ave., Newport News, VA 23606, USA*
[b]*University of New Hampshire, Durham, NH 03824, USA*
[c]*The College of William and Mary, Williamsburg, VA 23185, USA*
[d]*Christopher Newport University, Newport News, VA 23606, USA*
[e]*Virginia Polytechnic Institute and State University, Blacksburg, VA 24061, USA*
[f]*CEA Saclay, F-91191, France*
[g]*Kyungpook National University, Taegu, 702-701, South Korea*
[h]*Rice University, Houston, TX 77251-1892, USA*
[i]*University of Virginia, Charlottesville, VA 22901, USA*

Received 10 March 1999

Abstract

The time of flight system for the CEBAF Large Acceptance Spectrometer (CLAS) at the Thomas Jefferson National Accelerator Facility is described. The system, covering an area of 206 m^2, is composed of scintillation counters 5.08 cm thick, 15 and 22 cm wide, and lengths which vary from 32 cm at the most forward angle to 450 cm at larger angles. All of the components of the system have been designed to optimize the time resolution. Event timing, achieved by leading-edge discrimination with time-walk correction, has been measured with cosmic rays, a laser pulser, and known particle interactions. The intrinsic time resolution varies from about 80 ps for the short counters to 160 ps for the longer counters. Reconstruction of interacting particles during the first period of operation yields an average time resolution for electrons of 163 ps.

PACS: 29.40.Mc

Keywords: CLAS; Time of flight; Plastic scintillator; Particle identification

* Corresponding author. 12000 Jefferson Ave., Newport News, VA. Tel.: + 1-757-269-7625; fax: + 1-757-269-5800.
E-mail address: elton@jlab.org (E.S. Smith)
[1] Present address: 17 Pinewood Rd, Peabody, MA 01960, USA.
[2] Present address: Institut de Physique Nucléaire, F-91406 Orsay, France.
[3] Present address: Physics Dept., Tulane University, New Orleans, LA 70118, USA.
[4] Present address: 5 Crockett St, Rochester, NH 03867, USA.
[5] Present address: MIT-Bates Linear Accelerator Center, Middleton, MA 01949, USA.
[6] Present address: Lucent Technologies, Holmdel, NJ 07733-3030, USA.

0168-9002/99/$ - see front matter
PII: S0168-9002(99)00484-2

1. Overview of CLAS

The CEBAF Large Acceptance Spectrometer (CLAS) is a magnetic toroidal multi-gap spectrometer at the Continuous Electron Beam Accelerator Facility (CEBAF) at the Thomas Jefferson National Accelerator Facility in Newport News, Virginia. The magnetic field is generated by six superconducting coils arranged around the beam line to produce a field, primarily in the azimuthal direction about the beam axis, with a maximum intensity of about 2 T. The size and the shape of the coils, about 5 m long and 2.5 m wide, were chosen to optimize the physics program for fixed targets with electron beams of a few GeV.

The CLAS detector package consists of drift chambers to determine the paths of charged particles, gas Cherenkov counters for electron identification, scintillation counters for measurement of time of flight (TOF), and an electromagnetic calorimeter to identify showering particles such as electrons and photons. The trigger is formed using fast coincidences between the Cherenkov counters, TOF counters or electromagnetic calorimeters. The six sectors between the coils are individually instrumented to form six independent magnetic spectrometers. A plan view of the particle detection system is given in Fig. 1, and a view in the direction of the beam (cut at the target region) is shown in Fig. 2.

2. Design of the time-of-flight system

The requirements for the TOF system include excellent timing resolution for particle identification, and good segmentation for flexible triggering and prescaling. The design parameters were chosen

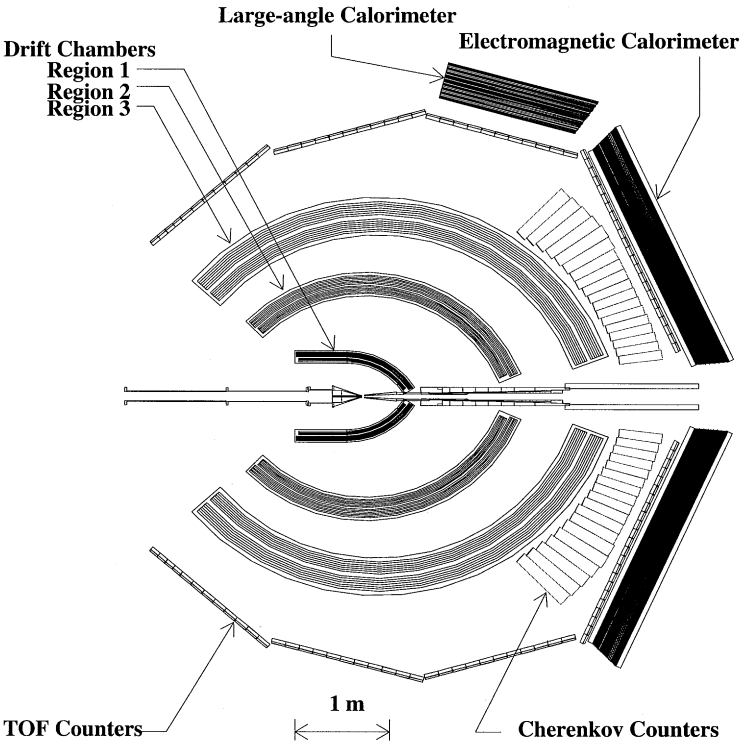

Fig. 1. Midplane slice of the CLAS detection system (plan view). The Cherenkov counters and the electromagnetic calorimeter extend to 45°. The electron beam is incident from the left.

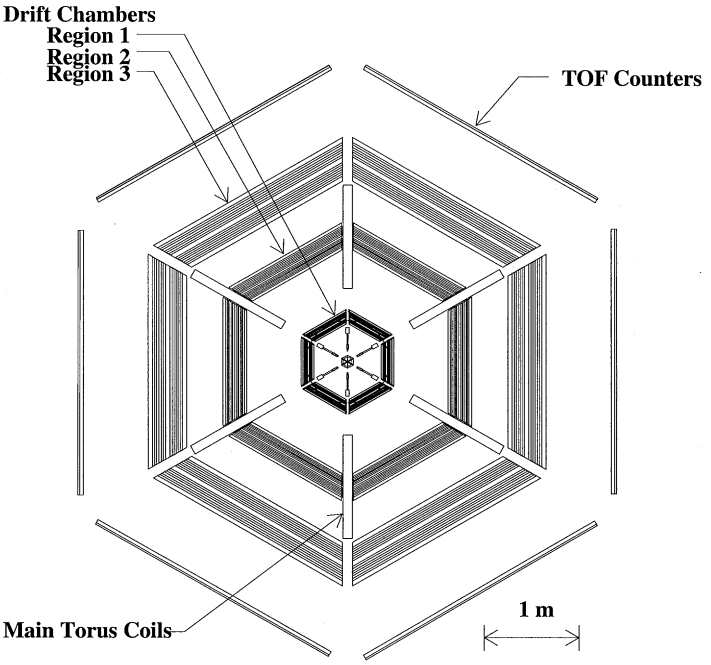

Fig. 2. Cross section view of CLAS, cut through the target. Shown are the cryostats of the superconducting magnet which slice the detector into six sectors, drift chambers, and TOF scintillators.

to allow separation of pions and kaons up to 2 GeV/c. The most energetic particles are produced at small angles. The system specifications called for a time resolution of $\sigma = 120$ ps at the smallest angles and 250 ps at angles above 90°. Particle identification is achieved by off-line analysis that combines leading-edge time measurements with pulse-height information for time-walk corrections.

The discriminated scintillation counter signals can also be used in the CLAS Level 1 trigger. The system must, therefore, provide signals representing a uniform response and adequate granularity to select particles reaching the TOF detectors. The timing in the trigger hardware is limited by flight-time variations between fast (e.g. electrons) and slow particles (protons with momenta of 300 MeV/c or less) which can be as large as 50 ns. Therefore, precise timing information is only achieved in off-line software analysis using the momentum and position measured with the drift chambers.

The TOF system is also used for energy-loss measurements and velocity determination in specific instances. Pulse-height information, being proportional to the energy loss in the counter, provides an independent means for the identification for slow particles. Also, the flight time can provide a more accurate measurement of particle energy than magnetic analysis for slow particles when the tracking resolution is dominated by multiple scattering. The momentum of 500 MeV/c protons can be determined with comparable uncertainty using either time of flight or magnetic analysis. If neutrons interact in the counters (efficiency $\sim 5\%$), their energies can only be determined by time of flight.

The system must also be capable of operating in a high-rate environment. The maximum counting rate in an electron beam occurs in the forward direction where, at a luminosity of 10^{34} cm^{-2}s^{-1}, the average rate per scintillator is approximately 100 kHz. Fig. 3 shows the measured rates for counters at different angles.

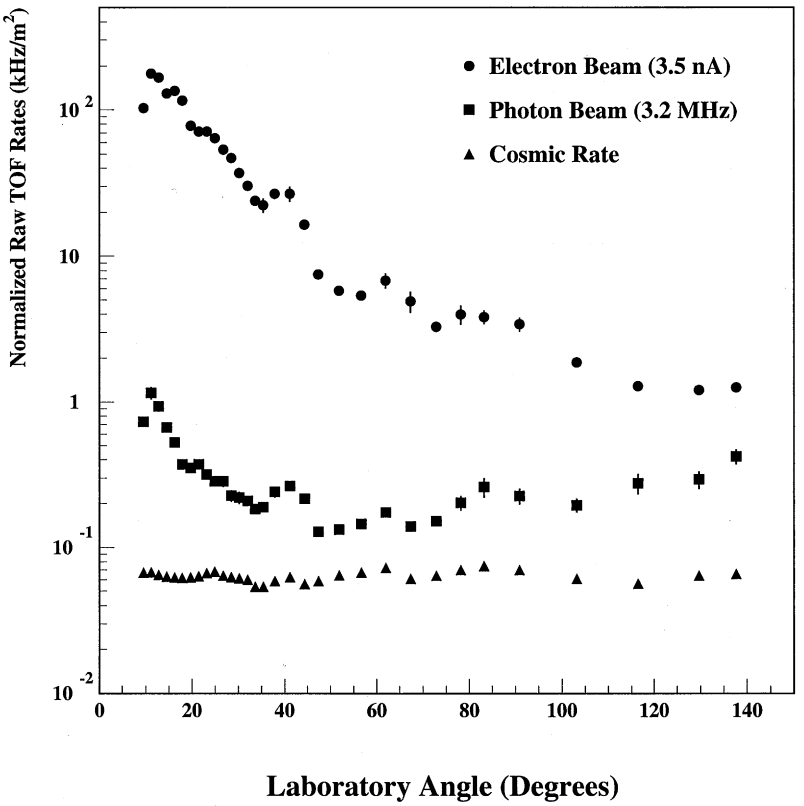

Fig. 3. Typical rates in the TOF counters as a function of angle for different running conditions: (a) electron beam of luminosity 3×10^{33} $cm^{-2}s^{-1}$ and 100 mV discriminator threshold and (b) photon beam with a prescaled trigger rate of 3.2×10^6 s^{-1} and a 200 mV threshold. The photon flux in the tagged range was three times higher.

In order to meet the requirements, the major considerations in the design of the TOF system were:

(1) *Geometry*. The projected space behind the superconducting coils of the CLAS detector is inactive and therefore useful for locating light guides, photomultiplier tubes (PMTs), voltage dividers, and cables. The remaining space is the fiducial volume of the detector and was covered with scintillator material. This active region corresponds to scattering angles from 8° to 142° and a total area of 206 m^2.
(2) *Size*. The width of each scintillator determines the granularity of the scattering angle definition in the trigger. Also, the overall size of the system demanded careful consideration of light collection in order to optimize the time resolution of the system.
(3) *Magnetic field*. The PMTs had to be properly shielded from the stray magnetic fields of the CLAS torus.
(4) *Crossing tracks*. Since particle trajectories can intersect adjacent TOF counters, light from both counters must be summed for separation from background and particle analysis.
(5) *Readout capability*. The design goal of CLAS is to record events at a continuous rate of up to 1500 Hz. At this rate, conversion times of 30 μs contribute 5% to the dead time.

Each component was considered within the context of these design constraints, and optimized against cost considerations. The time resolution is

determined by various factors. Limitations in the electronic measurements and systematic corrections yield a constant contribution independent of the details of the counter geometry or construction. Statistical contributions come from the generation of light, both from the intrinsic light yield of the scintillator itself as well as from the transit time of particles through the counter. The light is then transported to the photomultiplier tubes. Some of the light is lost due to attenuation and also dispersed in time by taking different paths from the impact point to the PMT. The response of the PMT, especially variations across the photocathode, further disperse the photon arrival times. These are folded with the intrinsic response of the electronic gain of the PMT to produce a pulse which is used for the time measurement. Finally, the dispersion of the signal in cables and time-walk in the discrimination of the pulse are important effects that must be addressed to achieve sub-nanosecond resolution.

The selected design is based on long rectangular plastic scintillators, each with two PMTs, one on each end. Several systems, similar to the one we describe here, have achieved timing resolutions $\sigma \sim$ 100–200 ps [1–11,13,14]. A comparison is given in Table 1, which lists systems in order of counter length. The performance of these TOF systems is limited by the number of photoelectrons that are collected [15] and dispersion due to counter length. Therefore, the best resolution is obtained with short counters with low dispersion and attenuation, thick counters which produce more photoelectrons for an incident particle, and narrow counters which closely match the photocathode. Thick counters also provide a larger signal for minimum-ionizing particles, thus improving the separation of events from background.

3. Description

3.1. Geometry

The inactive components of the detector are constrained to fit in the projected space behind the superconducting coils. The scintillators are positioned outside the tracking system between the Cherenkov counters and the calorimeter. The counters are mounted in four panels in each of the six sectors. Scintillators 1–23 are mounted in panel 1, and are referred to as "forward-angle" counters. They correspond to scattering angles less than 45°. Panels 2, 3 and 4 are called "large angle". Details of the configuration are given in Tables 2–4. The nominal thickness of 2 in. (5.08 cm) is uniform throughout, chosen to give a large signal for traversing minimum-ionizing particles compared to background. At forward angles, this thickness was also chosen to optimize geometric matching to a 2-in.

Table 1
Comparison of time resolution for different detector systems

Detector	Scintillator	Length (cm)	Width (cm)	Thickness (cm)	Phototube	σ (ps)
CERN [1]	NE102A	25	8	2	Philips XP2020	123
DASP [2]	NE110	172	20	2	RCA 8575	210
E813 [3]	BC408	200	8.5	5	Hamamatsu H1949	110
ARGUS [4]	NE110	218	9.3	2	RCA 8575	$\sim$ 210
CLEO II [5]	BC408	280	10	5	Amperex XP2020	139[a]
OBELIX [6]	NE110	300	$\sim$ 9.3	4	Philips XP2020	170
E735 [7]	BC408	305	10	5	Philips XP2020	110[b]
MARK III [8]	NE Pilot F	317.5	15.6	5.1	Amperex XP2020	$\sim$ 171
DELPHI [9,10]	NE110	350	20	2	EMI 9902KB	1200[c]

[a] 110 ps reported by Giles et al. [11].
[b] 140 ps reported by Alexopoulos et al. [12].
[c] The large time spread measured in the DELPHI detector is due to substantial light loss in the 180° bend of its light guides.

Table 2
Dimensions of forward-angle scintillators in the time-of-flight system. All scintillators are nominally 5.08 cm thick

Scintillator number	Width (cm)	Length (cm)	Light guide configuration	PMT	Nominal lab angle (deg)	Nominal distance from target (cm)
1	15	32.3	Straight	EMI9954A	8.6	513
2	15	48.1	Straight	EMI9954A	10.3	509
3	15	64.0	Straight	EMI9954A	11.9	506
4	15	79.8	Straight	EMI9954A	13.6	503
5	15	95.7	Straight	EMI9954A	15.3	500
6	15	106.6	Straight	EMI9954A	17.0	498
7	15	122.4	Straight	EMI9954A	18.8	496
8	15	138.3	Straight	EMI9954A	20.5	495
9	15	154.1	Straight	EMI9954A	22.3	494
10	15	170.0	Straight	EMI9954A	24.0	493
11	15	185.8	Straight	EMI9954A	25.8	493
12	15	201.7	Straight	EMI9954A	27.6	494
13	15	217.6	Straight	EMI9954A	29.3	495
14	15	233.4	Straight	EMI9954A	31.1	496
15	15	249.3	Straight	EMI9954A	32.8	498
16	15	265.1	Straight	EMI9954A	34.5	501
17	15	281.0	Straight	EMI9954A	36.2	504
18	15	296.8	Straight	EMI9954A	37.9	507
19	15	312.7	Straight	EMI9954A	39.6	511
20	15	328.5	Straight	EMI9954A	41.2	515
21	15	344.4	Straight	EMI9954A	42.8	519
22	15	360.2	Straight	EMI9954A	44.4	524
23	15	376.1	Straight	XP2262	45.9	529

Table 3
Dimensions of the single large-angle scintillators in the time-of-flight system. All scintillators are nominally 5.08 cm thick

Scintillator number	Width (cm)	Length (cm)	Light guide configuration	PMT	Nominal lab angle (deg)	Nominal distance from target (cm)
24	22	371.3	Bent	XP4312B/D1	47.4	514
25	22	378.2	Bent	XP4312B/D1	49.6	504
26	22	385.0	Bent	XP4312B/D1	51.9	495
27	22	391.9	Bent	XP4312B/D1	54.3	487
28	22	398.7	Bent	XP4312B/D1	56.8	480
29	22	405.6	Bent	XP4312B/D1	59.4	473
30	22	412.5	Bent	XP4312B/D1	62.0	468
31	22	419.3	Bent	XP4312B/D1	64.7	463
32	22	426.2	Bent	XP4312B/D1	67.4	460
33	22	433.0	Bent	XP4312B/D1	70.2	458
34	22	439.9	Bent	XP4312B/D1	72.9	457
35	22	445.1	Bent	XP4312B/D1	75.7	457
36	22	439.3	Bent	XP4312B/D1	78.2	446
37	22	433.6	Bent	XP4312B/D1	80.8	437
38	22	427.8	Bent	XP4312B/D1	83.5	428
39	22	422.0	Bent	XP4312B/D1	86.3	421

Table 4
Dimensions of paired large-angle scintillators in the time-of-flight system (see Section 3.4.7). All scintillators are nominally 5.08 cm thick

Scintillator number	Width (cm)	Length (cm)	Light guide configuration	PMT	Nominal lab angle (deg)	Nominal distance from target (cm)
40a	22	416.3	Bent	XP4312B/D1	89.3	414
40b	22	410.5	Bent	XP4312B/D1	92.2	409
41a	22	404.8	Bent	XP4312B/D1	95.3	405
41b	22	399.0	Bent	XP4312B/D1	98.4	402
42a	22	393.3	Bent	XP4312B/D1	101.6	400
42b	22	387.5	Bent	XP4312B/D1	104.8	399
43a	22	380.1	Bent	XP4312B/D1	108.8	402
43b	22	363.5	Bent	XP4312B/D1	112.0	395
44a	22	347.0	Bent	XP4312B/D1	114.9	389
44b	22	330.4	Bent	XP4312B/D1	118.1	384
45a	22	313.9	Bent	XP4312B/D1	121.4	381
45b	22	297.3	Bent	XP4312B/D1	124.7	378
46a	22	280.8	Bent	XP4312B/D1	128.0	377
46b	22	264.2	Bent	XP4312B/D1	131.4	378
47a	15	246.8	Straight	XP2262	134.2	379
47b	15	235.4	Straight	XP2262	136.5	380
48a	15	224.0	Straight	XP2262	138.8	383
48b	15	212.7	Straight	XP2262	141.0	385

PMT. Each scintillator is placed perpendicular to the direction of incident beam such that the width of the counter subtends about 2° of the scattering angle. The counters are parallel to the normal drift chamber wires and span the azimuthal angular range of one sector.

The choice of counter width was a compromise between cost and time resolution, with many possible options. If a large width is used, a given area can be covered by fewer phototubes, but the light guide design becomes more complicated and costly, especially if coupled to 2-in. PMTs. To ease the fabrication, assembly and testing of a large number of counters, we chose to build the system based on two widths. We selected 15-cm-wide scintillators and 2-in. PMTs for the forward-angle system due to space constraints. For the large-angle system, a 22-cm width coupled to bent and twisted light guides and 3-in. PMTs was selected.

Each of the six sectors has 57 scintillators with a PMT at each end. The last 18 of these are paired into nine logical counters, each with an effective width of 44 cm (see Section 3.4.7). This grouping results in the system having a total of 48 logical counters per sector. The lengths of the counters vary from 32 to 445 cm. A view of the counters in one sector is shown in Fig. 4.

3.2. Components

3.2.1. Scintillation material

To optimize the time resolution over the volume of the counter, a scintillation material with fast time response and low light attenuation was needed. Since almost 80% of the area covered by the CLAS TOF scintillators requires lengths greater than 300 cm, limitations due to fabrication of long pieces were also an important consideration.[7] Measurements of the effective attenuation were performed on 5-cm-thick scintillators, 10–20 cm wide, and typically 300 cm long [16]. The effective attenuation length differs from the bulk attenuation length due to imperfect reflectivity and also due to

[7] We performed some tests of scintillators bonded together to produce long counters. The attenuation and absolute output at the joint were initially satisfactory. However, later tests showed a deterioration of 10–15% in the measured attenuation length and visual inspection revealed some crazing along the joined surfaces.

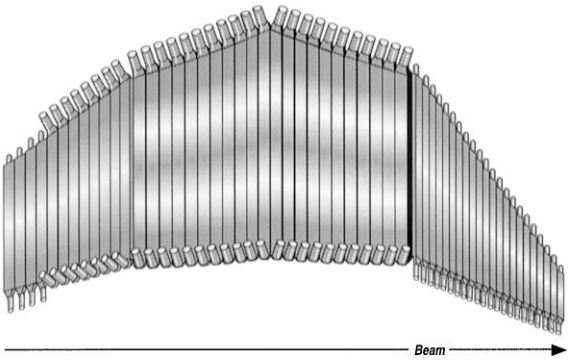

Fig. 4. View of TOF counters in one sector showing the grouping into four panels. The forward-angle scintillators (panel 1) have short stubby light guides and 2-in. PMTs. The large-angle system, except for the last four counters, has bent light guides coupled to 3-in. PMTs.

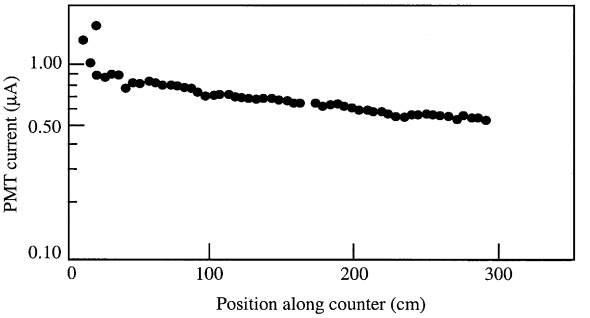

Fig. 5. The light-attenuation curve for a $300 \times 20 \times 5$ cm^3 piece of BC-408 scintillator. The measured effective attenuation length, 500 cm, was determined by moving an X-ray source along the length of the counter.

the presence of light reflected from the opposite light guide and PMT. Bicron[8] BC-408 scintillator yielded a single attenuation component of 500 cm, as shown in Fig. 5. Bicron was also able to fabricate scintillator pieces as long as 450 cm. Based on these considerations, we selected Bicron BC-408 for the scintillator material. Bicron specifies the following characteristics for the scintillator: light output (64% of anthracene), rise time (0.9 ns), decay time (2.1 ns), and wavelength of maximum emission (425 nm).

3.2.2. Photomultiplier tubes

3.2.2.1 Forward-angle counters. A cost-effective solution to cover a large area, while maintaining good time resolution, was achieved by using 2-in. diameter, 12-stage PMTs. The forward-angle TOF system makes use of 2-in. PMTs each having a 15.9 cm^2 photocathode area which covers the 76.2 cm^2 cross-sectional area of the scintillator. Four comparable PMT types from EMI (9954B05),[9] Amperex (XP2262), Burle (8575) and Hamamatsu (R329) were tested for their time performance [17,18]. Two samples were obtained from the company, and, when available, we used the high-voltage divider network recommended by the company for the tube they provided.

To produce light with the correct frequency spectrum, a nitrogen laser was used to excite a small piece of BC-408 scintillator, which illuminated the entire photocathode. The intensity of light was varied systematically with five neutral density filters, covering the range from 40 to 340 photoelectrons. This was the range of light expected for minimum-ionizing particles traversing the center of the TOF counters. A fast signal (rise time ≤ 1 ns) from a photodiode was used to determine the time of the laser pulse. The PMT signals were discriminated with a Phillips [10] 715 constant-fraction discriminator. The time resolutions were determined by the variation of each PMT signal time relative to the photodiode reference. These are given in Table 5 along with measurements quoted in Ref. [11].

The Thorn EMI 9954A was selected for the forward-angle TOF system on the basis of cost. Each of the 318 photomultiplier tubes purchased was tested for rise time, gain, dark current and time resolution [19]. The gain variation among tubes was determined, with some tubes having as much

[8] Bicron Corporation, 12345 Kinsman Road, Newbury, OH 44065-9677, USA.

[9] EMI 9954B PMTs selected for high values of single electron resolution. The peak-to-valley ratios of the single electron spectrum for the tubes tested were 2.5 and 2.1.

[10] Phillips Scientific, 150 Hilltop Road, NJ 07446, USA.

Table 5
Time resolution obtained for different PMTs. The time resolution is quoted for 200 photoelectrons for the reference PMT. The actual number of photoelectrons for each PMT would vary depending on the value of its quantum efficiency

PMT	Measured rise time (average) 10–90% (ns)	σ (ps) (CLAS prototyping)	σ (ps) Ref. [11]
Amperex XP2020	—	95	115
Amperex XP2282B	—	95	—
Amperex XP2262	3.0	111	119
Burle 8575	3.0	144	140
Hamamatsu R329	4.0	103	—
EMI 9954	3.3	101	151[a]

[a]Measured EMI 9814, which has a lower sensitivity than the EMI 9954.

as a factor of ten difference in gain for a given voltage.

3.2.2.2. Large-angle counters. As the scattering angle increases, fixed angular increments in the center-of-mass system subtend larger angles in the laboratory, thus reducing the requirement for angular resolution of the scintillators at large angles. At the same time, typical particles detected at the large angles have longer flight times and, therefore, the requirements for time resolution are reduced. Consequently, the width of the counters at large angles (45–142°) was increased to 22 cm. The resolution, however, is limited by the light collection efficiency of the light guide, so PMTs of 3-in. diameter were considered for this application. This results in a photocathode area of 30.2 cm^2 for 111.8 cm^2 of scintillator cross section. The following four 3-in. tubes were considered: Thorn EMI 9821B, Philips[11] XP2312B and XP4312B/D1, and Hamamatsu H5540.[12] The Philips XP4312B/D1 was selected because of cost and its small transit-time variations measured across the face of the photocathode.

3.2.2.3. PMT Transit time. The relative transit times of the PMTs were measured by illuminating a small area of the photocathode with a fiber light source. Typical data for transit time shifts for 2-in. PMTs are shown in Fig. 6. The measured horizontal and vertical scans of the transit time were used to calculate the standard deviation of the time spread of PMT pulses for uniform illumination under the assumption of azimuthal symmetry. (This is an estimate of σ_{PMT} in Eq. (6); see Section 4.1.5.) While this assumption is not valid a priori, scans across different diameters yield similar values for the computed standard deviation. The computed value for the EMI 9954A was 0.55 ns [20].

The relative transit times of the 3-in. PMTs were measured in a similar manner. Fig. 7 shows the pulse height and time response of the Philips XP4312B tube for two orthogonal scans across the cathode. The variation computed from scans along two perpendicular directions was 0.07 and 0.24 ns for the central two inches along a diameter, and 0.32 and 0.34 ns for the full cathode. These small transit time differences contribute to improved time resolution of the counters at large angles.

3.2.3. Voltage divider

The schematic diagram of the high-voltage divider for the 2-in. tube is shown in Fig. 8 [21]. The divider for the 3-in. tube used similar concepts in its design [22]. Both dividers use four high-voltage field effect transistors (FETs) to fix the PMT gain by stabilizing the voltage and to protect the PMT against high light levels by shutting down the circuit in case of over-current. This stabilization scheme acts only on changes induced by signal currents from the dynodes and does not fix the voltage differences between dynodes, as zener

[11] Philips Components, 100 Providence Pike, Slatersville, RI 02876, USA.

[12] The H5540 is the voltage divider and magnetic shield assembly containing the R5004 PMT.

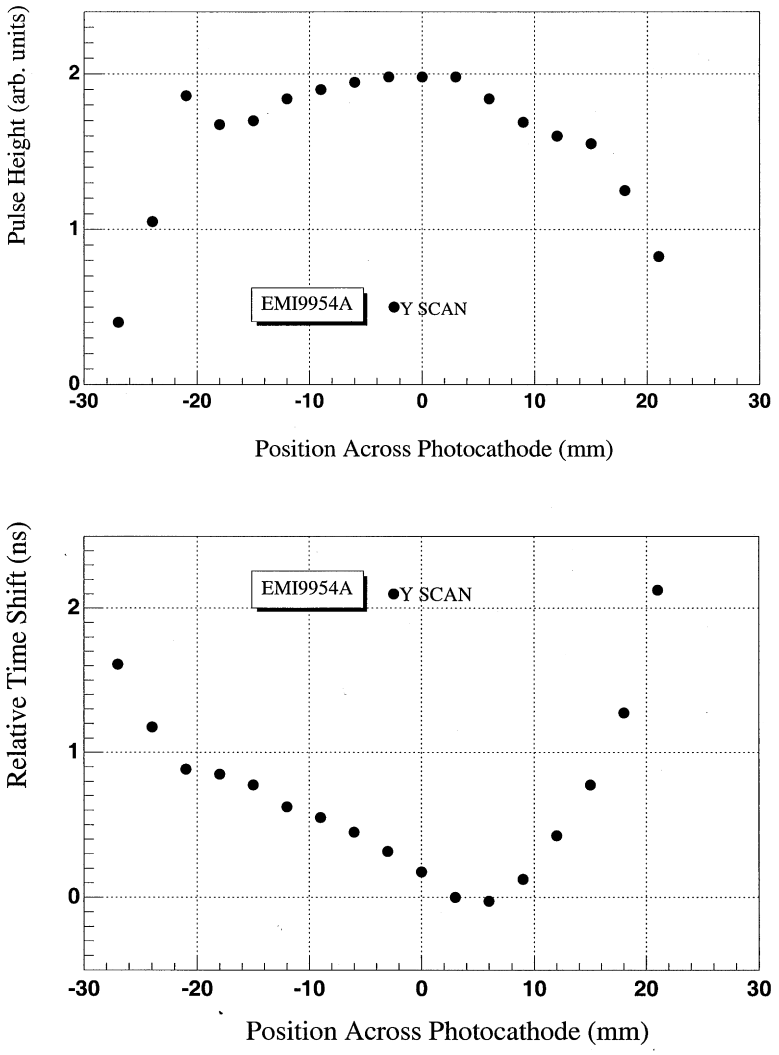

Fig. 6. Transit-time and pulse-height variations for the 2-in. Thorn EMI 9954A as measured by a fiber light source for different positions along the diameter of the photocathode.

diodes would. The FETs sense the current drain in the last four dynodes and shut down the PMT when the equivalent anode current exceeds about 300 μA. Fig. 9 shows that the anode signals are relatively insensitive to the total current drawn when compared to a conventional resistive base.

To optimize resolution, the grid voltage was varied. The best resolution was obtained when it was set equal to the first dynode voltage, as recommended by the manufacturer. The voltage ratio (dynodes 1–2)/(dynodes 2–3) gives an optimum resolution at 0.6, but is fairly constant for ratios between 0.4 and 1.5 so the manufacturer's specification of 1.0 was used. The cathode-to-first-dynode voltage was fixed by zener diodes at 480 V for the 2-in. divider whereas the 3-in. network has a 510 kΩ resistance between cathode and grid and 1570 kΩ resistance between the grid and first dynode. The voltages between the first dynode and the anode can be changed proportionally by varying the

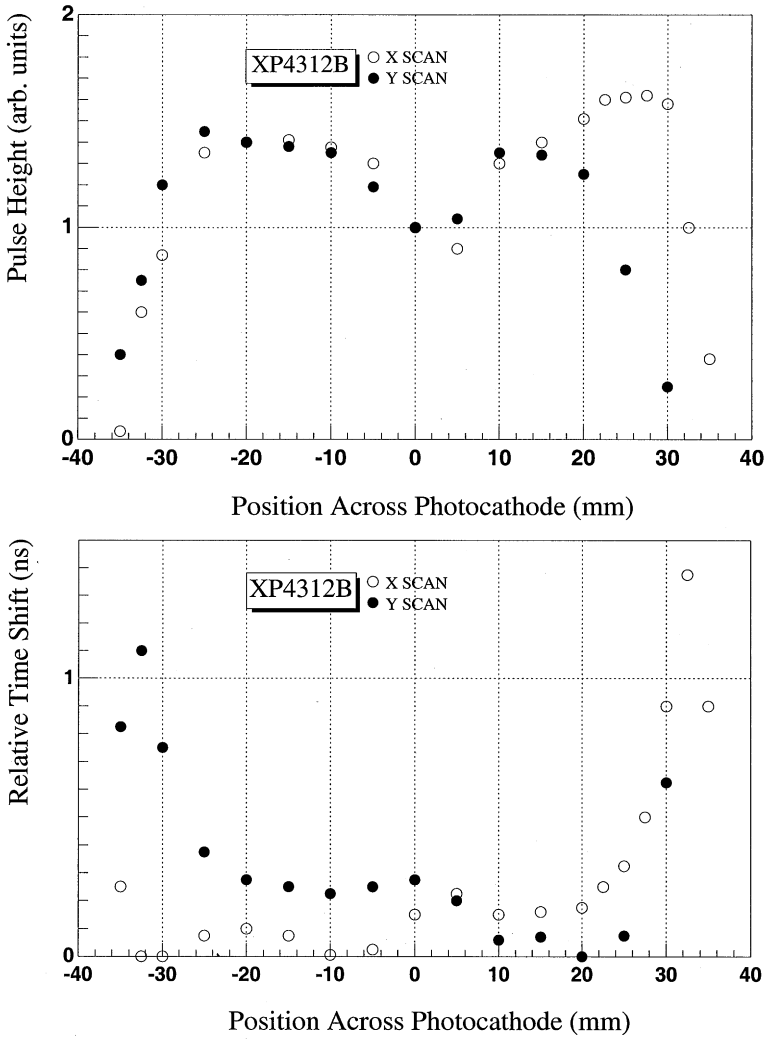

Fig. 7. Transit-time and pulse-height variations for the Philips XP4312B/D1 3-in. tube measured along two perpendicular diameters of the photocathode.

overall high voltage to compensate for gain variations among individual PMTs.

The tube-base assembly is shown in Fig. 10. In order to allow the scintillator to span the live area of the detector, the light guides, PMT and divider assembly were required to fit in the "shadow" of the magnet coils. To create as much space as possible for cables running between the TOF counters of adjacent sectors in CLAS, the high-voltage divider is of extremely compact design. Power consumption is approximately 1 W.

3.2.4. Light guides

The geometry of the CLAS detector leaves approximately 30 cm of space in the shadow of the coils at the ends of the TOF scintillators. Straight triangular light guides, 5 cm thick and tapering from the width of the scintillator down to the PMT,

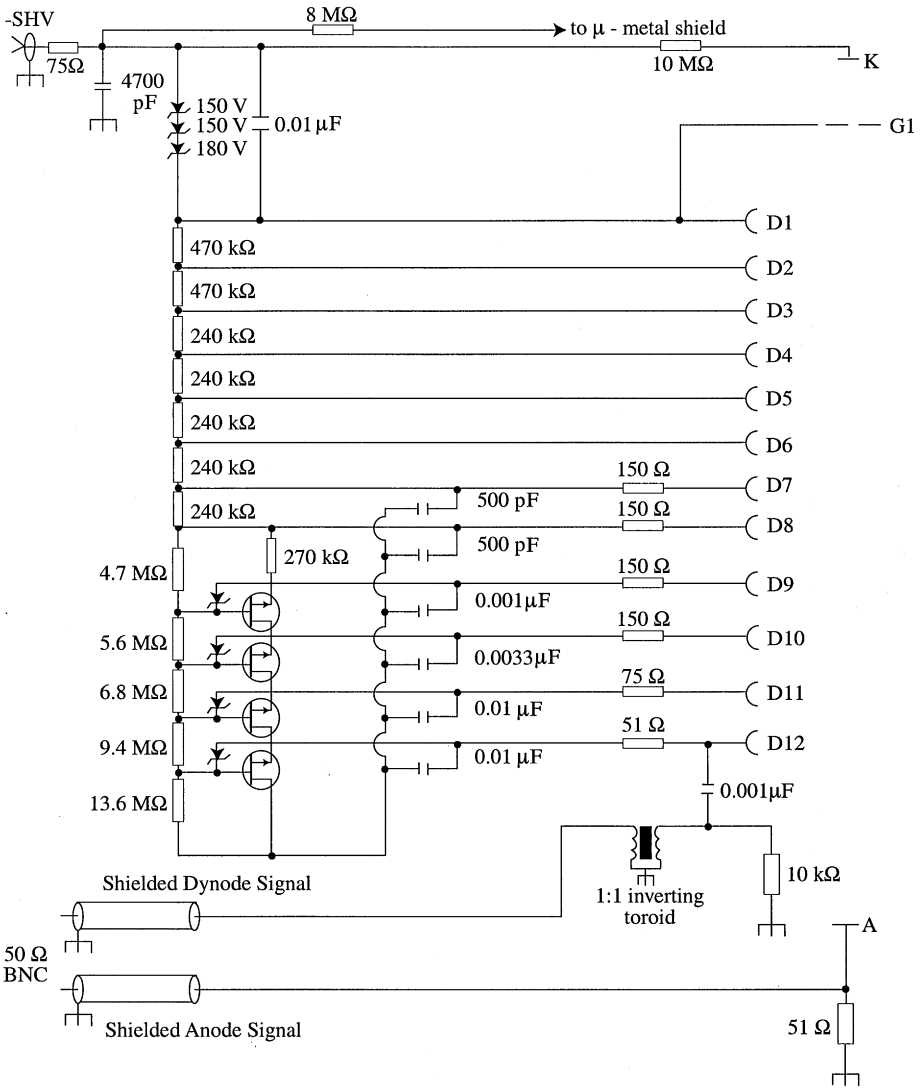

Fig. 8. Schematic diagram of the high-voltage divider for the EMI 9954A PMT. The last four stages of the divider are stabilized by high-voltage, field-effect transistors of type BSS-125. Diodes for dynodes 9–12 are of type 1N751 (4.7 V).

must have a length of less than 12 cm in order to fit the entire assembly into the allocated space. Because the magnetic field lines would then be aligned with the PMT, this configuration is difficult to shield magnetically. Nevertheless, such a design was selected for the forward-angle counters. The light guide consisted of a cylinder 4.5 cm in diameter and 6.2 cm long attached to a plastic trapezoid tapering from 15 to 4.5 cm over a distance of 5 cm. The purpose of this guide is to insure that a particle hitting anywhere in the scintillator has some solid angle for light transmission to the PMT. At the very least, the light guide allows more uniform light collection from tracks traversing the

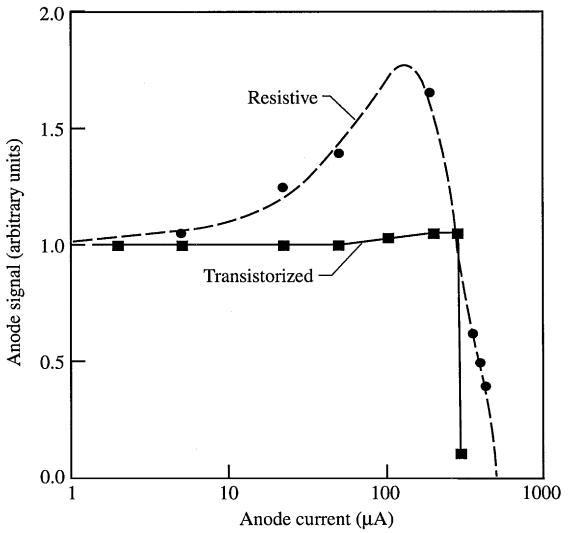

Fig. 9. The high rate capability of the transistorized network (Fig. 8) is shown here by plotting the measured pulse height for a constant light source as a function of input rate. For comparison we show the response of a typical resistor voltage divider.

near corners of the scintillator [23–25]. The sides of the wedge were painted black to minimize the reflection of light back to the opposite PMT.

For the large-angle counters, large areas were to be matched to the PMT, so we investigated designs which bent the light guides out of the plane of the scintillator. The timing properties of bent acrylic light guides have been considered previously. Some of the earliest work by Massam [26] concluded that less than 4% of light is lost if the bend radius is less than one-tenth of the acrylic thickness. Light guides made of thin sheets were used by a collider experiment at Fermilab [7]. These guides, with a 90° bend and made from seven lucite sheets, did not noticeably decrease the excellent timing resolution of their system.

Our design was developed by using the properties of the well-known light collectors invented by Winston [27]. These nonimaging collectors have the property of full collection efficiency up to a maximum angle (θ_{max}) of the incident scintillator light, with no collection efficiency beyond that angle. Historically, they have been used to minimize the photocathode coverage of Cherenkov detectors by optimizing the light collection. In that application the goal is to collect as much light as possible. For timing applications, the goal is to optimize the photocathode acceptance for prompt light. However, to make optimal use the photocathode coverage, a light guide for our application should preferentially discard late light which is incident at large angles. Thus, we studied Winston collectors which channel light at small angles relative to the scintillator axis. The traditional geometry for Winston collectors is a cone shape, which matches the shape of the photomultiplier tube, but does not fit the rectangular shape of the scintillator. For simplicity, we considered the projected profile of a Winston collector. In this case, the ideal collector constrains the entrance and exit apertures by the relation $w_g \geq w_s \sin\theta_{max}$. The apertures w_g and w_s correspond to either the widths or thicknesses of the light guide and scintillator, depending on the projection of interest. The length of the collector, l_c, is given by Eq. (1):

$$l_c \geq \tfrac{1}{2}(w_s + w_g)\cot\theta_{max}. \quad (1)$$

We note that the length of the collector scales with the size of the apertures, so one projection is proportional to the width of the scintillator and the other to the thickness. Ray-tracing calculations show that placing the collectors in series and replacing the optimal shapes with straight tapers is a useful approximation to the optimal solution. The final design for use with the 3-in. tube, illustrated in Fig. 11, consists first of a 6-cm wedge to reduce the thickness. The collection of light in the width dimension consists of two 30-cm-long bent acrylic pieces to better match the shape of the PMT and to fit within the allocated space in the detector. The simultaneous twist and bend of the 1.25-in.-thick acrylic has a compensating effect which reduces the distortion of the material. From Eq. (1), the lengths and apertures of these collectors are consistent with light collection at angles within 30° of the axis. The combination of all these considerations leads to an effective light collector for timing applications.

Ultraviolet-transmitting (UVT) acrylic was used for all light guides. Standard acrylic contains additives to reduce transmission in the UV, which over time can produce coloring, as demonstrated with studies of radiation damage [28]. Therefore, UVT

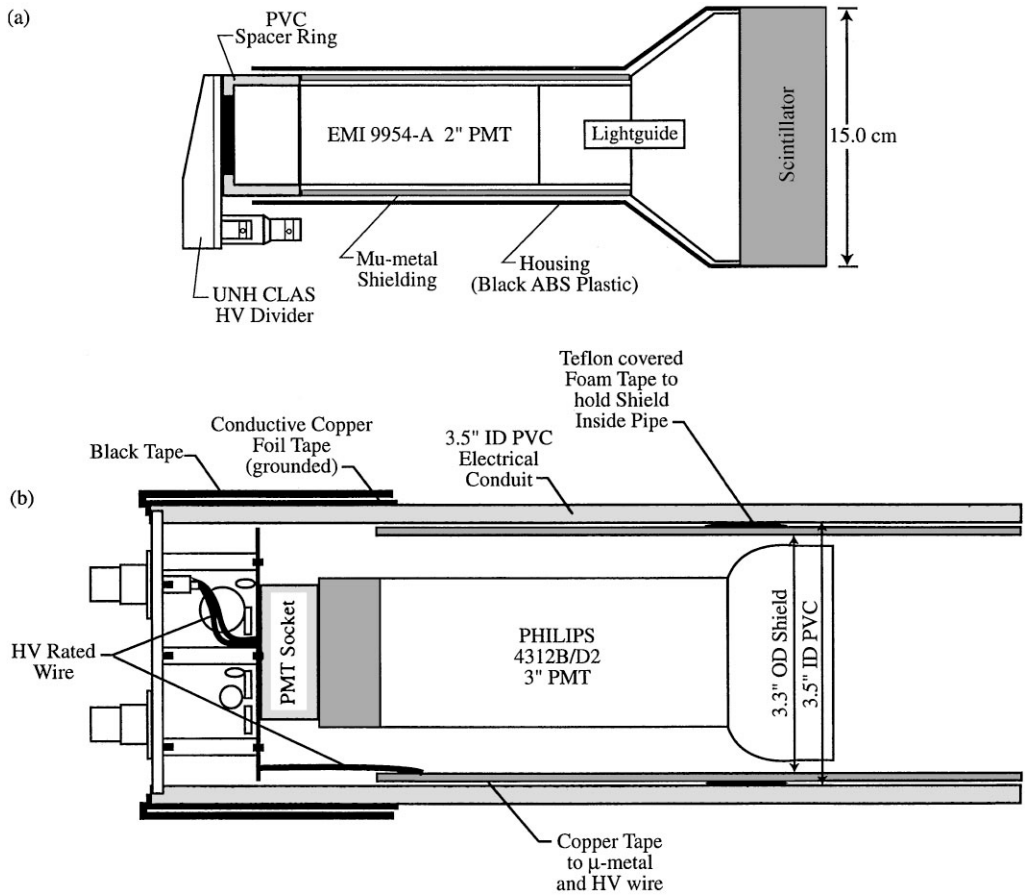

Fig. 10. Side view of the PMT base assembly mounted on a CLAS TOF scintillator. (a) The compact design is required by space limitations in the CLAS detector for 2-in. PMTs. (b) The curved light guide allows additional space for the 3-in. PMTs.

acrylic is expected to remain transparent longer than standard acrylic. The added cost of using UVT is small compared to the overall cost of the guide.

3.2.5. Magnetic shields

We studied the effects of magnetic fields on gain and time resolution for both the 2- and 3-in. PMTs [29,30]. We also investigated various magnetic shield geometries and orientations to determine how to shield the magnetic field to an acceptable level along the length of the PMT.

The CLAS TOF scintillator counters are located approximately 5 m from the target in a local magnetic field that is less than 10 (30) G at the location of the forward (large) angle PMTs. The magnetic shielding must reduce both the axial and transverse components of the field, especially near the photocathode, but the shield must also conform to the spatial requirements of the light guide and PMT assembly. At reaction angles of less than 45°, two-thirds of the field is axial, which produces a relatively smaller effect on PMT performance than the transverse component, but it is more difficult to shield.

3.2.5.1. Two-in. PMT. To determine the effects of magnetic fields on PMT response, output pulse heights for an unshielded PMT were measured in a purely axial as well as purely transverse magnetic field. The pulse height is only reduced by a factor of

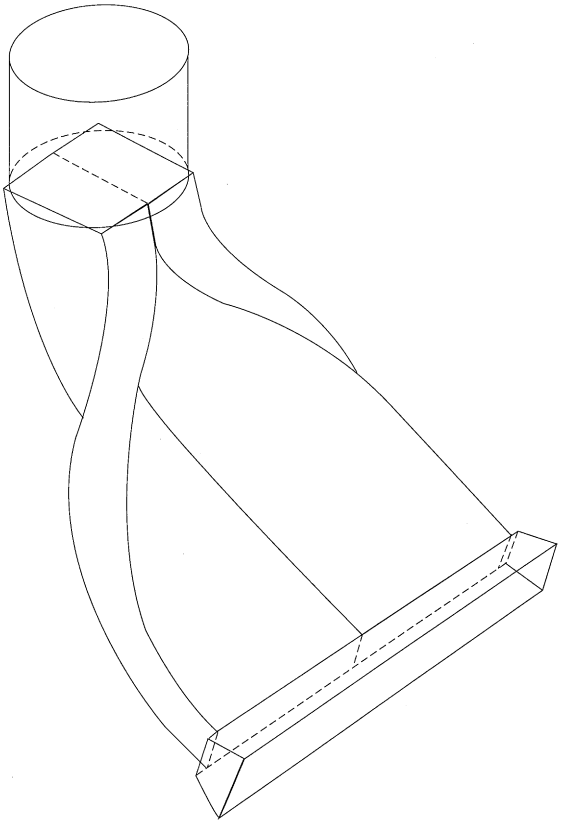

Fig. 11. Light guide used with the 3-in. phototubes for the large-angle counters. The bent light guide is required for efficient coupling of the 3-in. PMT to the 22-in.-wide, 2-in.-thick scintillator and to make available additional space for the PMT housing.

two in a purely axial field of 5 G. There is a much more dramatic reduction for transverse fields. The time resolution for an unshielded PMT was also measured in a purely axial and purely transverse magnetic field at two different light intensities. The time resolution is degraded as the field is increased, but the tests indicated that the time resolution of a PMT is not significantly degraded for fields less than 1 G.

A cylindrical shield is the most straightforward approach to magnetic shielding. In tests we determined that a single cylinder made from 0.020-in.-thick mu-metal is sufficient to shield an axial magnetic field in the region of the photocathode below 10 G. However, some PMTs are located in a region of slightly higher field, so we selected a mu-metal[13] shield 0.040 in. thick. The geometry of the shield is shown in Fig. 10a. The shield extends 2 inc. beyond the front face of the 2-in. PMT.

3.2.5.2. Three-in. PMT. The response of the XP4312B/D1 PMT was measured as a function of an external 20-G magnetic field perpendicular to the axis of the tube for several different shielding configurations. The two shields tested were cylindrical tubes 8.5- and 11-in. long, both 1 mm thick. The 11-in.-long cylinder adequately shielded the PMT from fields up to 20 G, but the 8.5-in. shield fell short. By scaling the measured magnetic field strength in the vicinity of the tube, we selected a 9.5-in.-long and 1.5-mm-thick cylinder to shield a 30 G field. The shield extends 2.5 in. beyond the photocathode (see Fig. 10b) and is fabricated with mu-metal material which was specified in the same way as for the 2-in. tubes.

3.3. Assembly

Each scintillation counter was individually wrapped, and assembled with two photomultiplier tubes and light guides, one at each end. The layers are shown in Fig. 12. The outer coverings of the scintillator plastic consist of two layers of aluminum foil surrounding the plastic, one strip of 0.005 in. lead foil on the side facing the target and finally one layer of black Kapton. The lead foil was placed to shield the scintillators from background X-rays produced in the target. This is the only extra material facing the target.

After wrapping, each scintillator was attached to a support structure, light guides and photomultiplier tubes were glued in place, and an optical fiber installed for the laser calibration system. Dymax 3-20262 UV-curing optical cement[14] was used as a bond for the guide-scintillator interface as well as the PMT-light guide interface. This cement cures in 15 min with exposure to a 15 W UV lamp. The light

[13] The mu-metal material was 80% nickel, high-permeability alloy conforming to MIL-N-14411 Type 1, hydrogen annealed with no special finish.

[14] Dymax Corporation, 51 Greenwoods Rd., Torrington, CT 06790. Curing time is reduced to several seconds with Dymax Light Weld UV lamps.

guides of several counters were originally bonded to the PMT with a hard cement. Breakage of some of these PMTs occurred due to temperature change, because the cement did not allow for sufficient differential expansion.

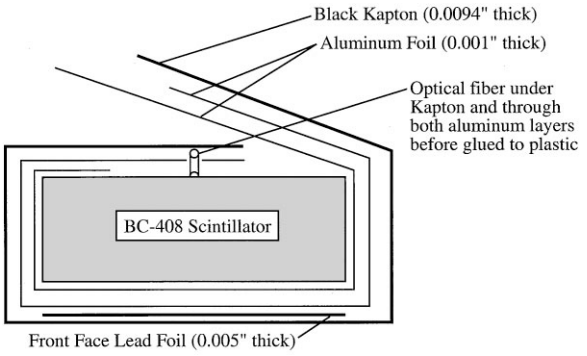

Fig. 12. Cross section of counter wrapping. The UV-transmitting fiber is placed under the Kapton and through both aluminum layers before being glued to the plastic. The lead foil is to absorb low-energy background X-rays from the target.

Each scintillation counter is supported individually by a composite sandwich structure of stainless steel skins on structural foam which is attached to the detector frame only at the two ends. The composite structure, which mounts on the scintillator side facing away from the target, provides uniform material encountered by scattered particles. The support was undersized so the counters could be placed as close together as allowed by the wrapping material. The assembly with support is shown in Fig. 13. The forward-angle counters were mounted on 1-in.-thick supports to minimize the thickness of the package. This thickness was adequate for static loads, but marginal for dynamic loading. The maximum deflection for installed scintillators is 4.4 mm, as estimated from deflections tests and the compound angle of each detector, which relieves the overall support requirements. The space for the large-angle counters allowed for 3-in.-thick sandwich supports which were mechanically much stiffer and resulted in no appreciable deflection. The counters were assembled at the University of New Hampshire and then transported to Jefferson Lab.

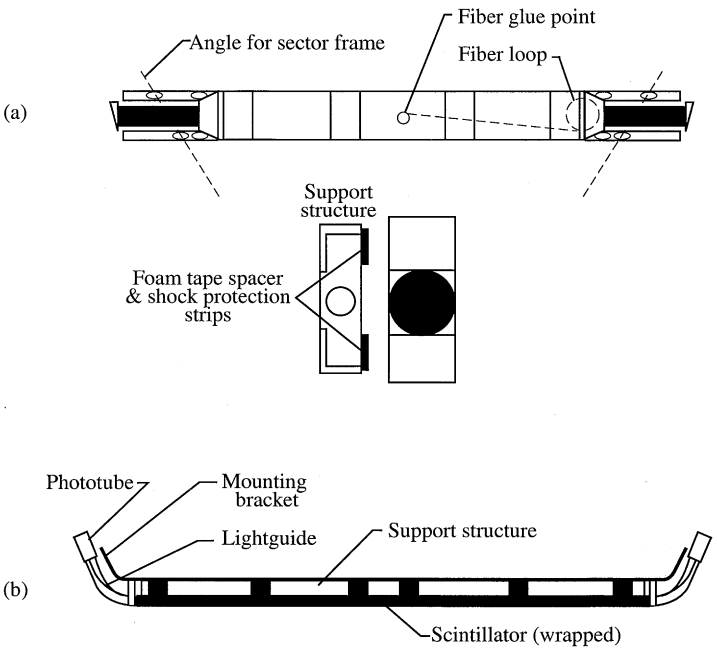

Fig. 13. Counter and support assembly. (a) Top view and enlarged end view of the forward-angle assembly. (b) Side view of the large-angle assembly.

3.4. Electronics

The TOF counters generate prompt signals for the CLAS Level 1 Trigger electronics [31] as well as signals for pulse-height and timing analysis. The overall layout of the TOF electronics which processes these signals is shown in Fig. 14. The trigger from the TOF counters is initiated by events that deposit energy in the scintillators greater than some preselected value. The PMT (inverted) dynode pulses go to a pretrigger circuit where two signals are produced. One of these signals goes to the Level 1 Trigger, and the second is a gate pulse which is used to accept the corresponding signals of the low-level discriminators. Custom electronics are used for energy discrimination in the pretrigger circuit. The charge of the anode pulse is recorded by a LeCroy 1881M ADC for later analysis. The time of the event is determined by a LeCroy 1872A FASTBUS TDC triggered by a LeCroy 2313 discriminator set at a low threshold for precise timing.

3.4.1. Cables

Fast timing of signals from the TOF system requires cables with low signal distortion. Measurements were made of the response of several types of coaxial cable, including RG-58, the usual cable for fast NIM electronics, RG-213 (formerly RG-8A/U) and Belden 9913, a low-loss semi-solid polyethylene cable. The lengths of the cables ($\sim$ 400 ns) were chosen to match the time required to form a first-level trigger for the CLAS detector. The response of the cables to a NIM logic signal, -0.75 V and 10 ns duration, was measured, and the transmission of pulses through the cable was simulated using a formalism developed by Fidecaro [32,33] (see Fig. 15). Note that the cable dispersion in high quality Belden 9913 is approximately equal to the dispersion in standard RG-213 cable for the same delay because the slower velocity in RG-213 ($\beta = 0.66$) compared to Belden 9913 ($\beta = 0.84$) compensates for the larger attenuation.

The effects of distortion on timing can be minimized by placing a discriminator very near the PMT. However, the cost of the system is increased by the need for a second discriminator to reshape the pulse at the input to the TDC. The slewing of the time, measured by a leading-edge discriminator as the pulse height is varied by $\pm$ 50%, is 1.15 ns for the pulse directly out of the photomultiplier,

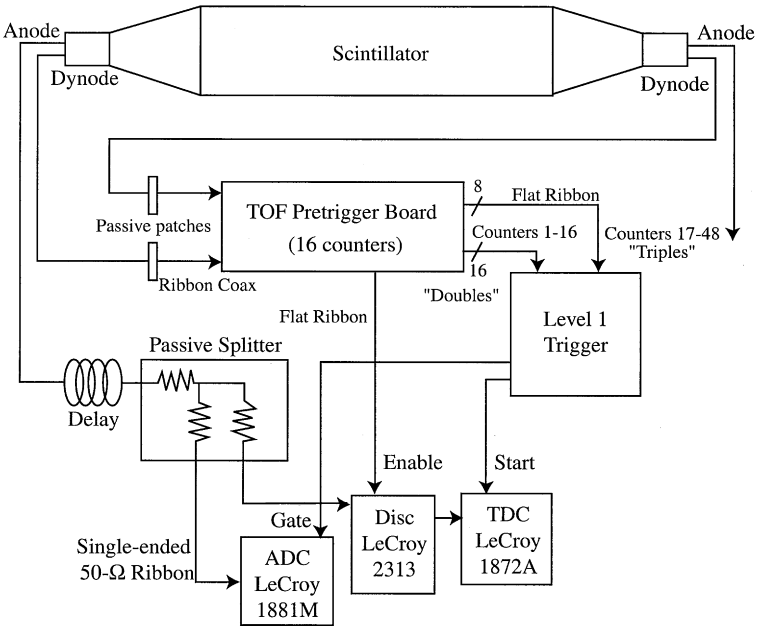

Fig. 14. Overall schematic of electronics for the TOF system. A diagram of the pretrigger board is given in Fig. 18.

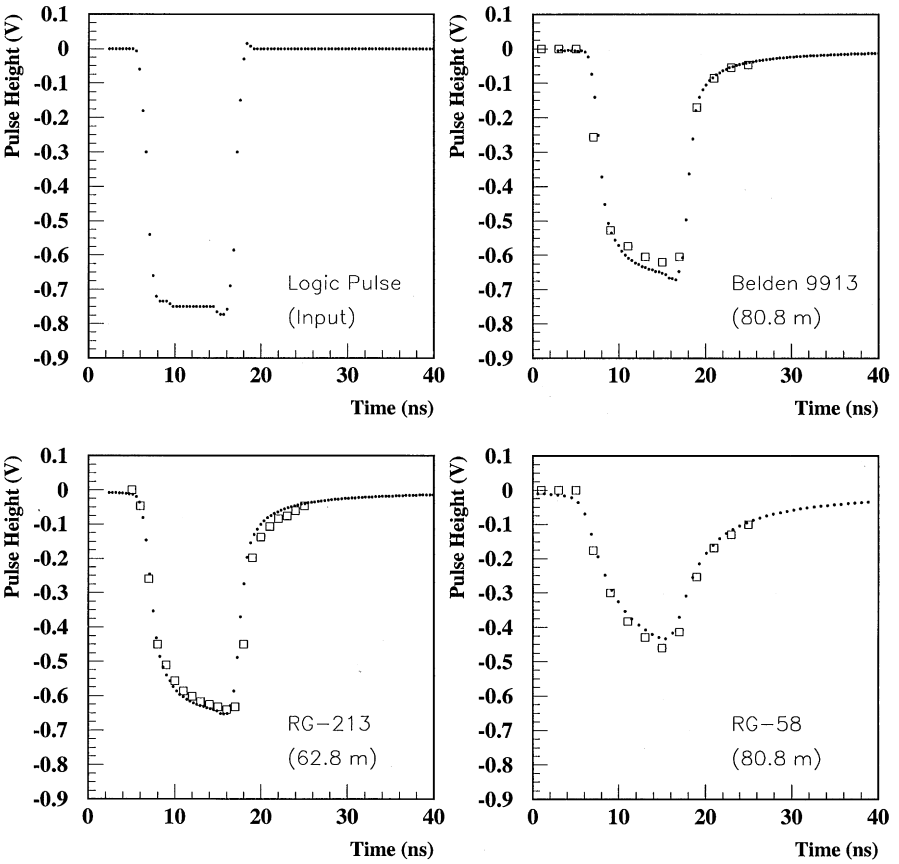

Fig. 15. Response of coaxial cables to a fast pulse. Comparison of a simulation (dotted lines) with measurements (squares) for three coaxial cables. The input pulse is a standard NIM logic signal 10 ns wide.

compared to 1.45 ns after the pulse is delayed by 100 m of RG-213 cable. This additional small difference contributes a negligible systematic uncertainty to the time-walk correction. On the basis of these considerations, we chose to use 17.7 m of Belden 9913 cable from the PMT dynode to the pretrigger board, and 83.8 m of RG213 from the anode to the ADC and discriminator. The faster trigger cables reduce the need for additional signal delay.

3.4.2. High-voltage supply

The photomultipliers for the TOF counters typically operate at about 2000 V with negative polarity. The maximum dark current drawn by the PMTs, on the assembled system, was 20 nA for the 2-in. tube and 30 nA for the 3-in. tube. The system is powered by five LeCroy 1458 mainframes which can contain up to 16 cards, each supplying 12 independent channels for a maximum of 192 channels per mainframe. The mainframes can be controlled by either an RS-232 port or a local area network. Control over the local area network is achieved by a Motorola MVME162 controller via ARCNET, a high-speed token-passing network protocol. A graphical user interface, using EPICS (Experimental Physics and Industrial Control System) running on a UNIX system, communicates via Ethernet with the Motorola controller.

3.4.3. Discriminator

A leading-edge, rather than a constant-fraction, discriminator was chosen for the system. Although a constant-fraction discriminator delivers better timing initially, off-line time-walk corrections to leading-edge time give comparable results at a significantly lower cost since the off-line analysis can use the measured charge [13]. CAMAC discriminators allow for remote control with fast inhibits at a low cost per channel.

In a system with many channels, the independence of neighboring channels is important. We found that older models of commercial discriminators failed to deliver the independence we required. The Phillips 7106 and LeCroy 4413 were tested to compare their use as a leading-edge discriminator. A check was made to see if the timing resolution of a channel could be degraded by activity in an adjacent channel. Fig. 16a plots the time shift in channel 1 measured when channels 2, 3, or 4 fire at

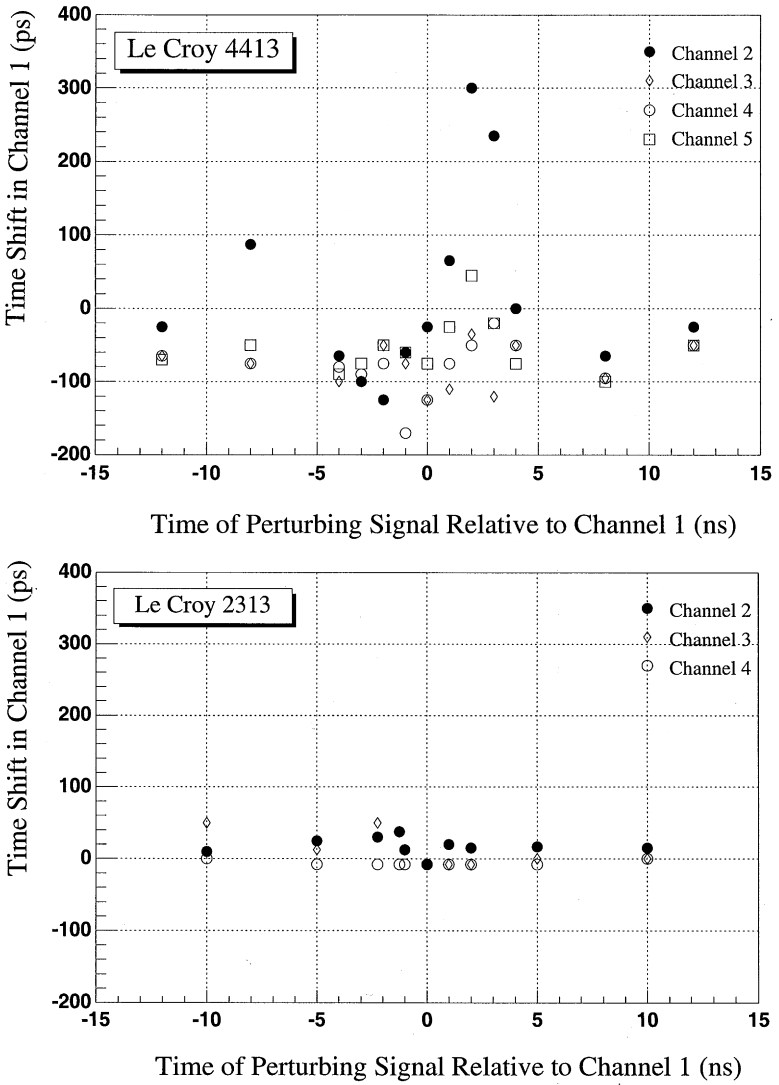

Fig. 16. The time shift in channel 1 is plotted as a function the time of adjacent firing channels for two 16-channel CAMAC discriminators, (a) LeCroy 4413 and (b) LeCroy 2313.

or near the same time for the LeCroy 4413 discriminator. (Similar results were obtained for the Phillips 7106 discriminator.) The test shows significant perturbations beginning at about + 5 ns and continuing to − 50 ns. Looking at channel 1, pulses in channel 2 caused the largest offsets, about 0.3 ns for a time difference of 2 ns. When other channels were pulsed, significant perturbations were limited to a narrow time window, less than 15 ns [34,35]. These shifts, which are significant for subnanosecond timing measurements, can be minimized by careful cabling, but it is highly desirable to use electronics which are immune to these problems.

The LeCroy 2313 leading-edge discriminator was designed with our specifications in mind, and finally chosen for the TOF system. This discriminator shows substantial reduction in the influence of neighboring channels. Fig. 16b shows that time shifts of less than 50 ps were measured under conditions similar to those of the 4413. The isolation is achieved by using one chip per discriminator channel.

3.4.4. Time-to-digital converter

Since the TOF system is designed to achieve time resolutions (σ) between 100 and 200 ps, the readout electronics had special timing requirements. The TDC must have root-mean-square sensitivities less than 50 ps in order to keep systematics from contributing more than 10% to the resolution of the final system. For maximum data rates of 1500 Hz, conversion times less than 30 μs were needed to keep the dead time below 5%.

The LeCroy 1872A Mod 100 time-to-digital converter (TDC) was selected for determining the time of phototube pulses. This unit is a 64-channel, 12-bit, single-width FASTBUS module. The original module had a fixed conversion time of 177 μs and did not satisfy the small conversion time requirement. A modified version, with a conversion time of 10 plus 2.7 μs per hit channel, significantly reduces the conversion time for the sparse data expected. The flight-time differences between protons and electrons over the acceptance of the detector is approximately 100 ns. The flight time for neutrons with momentum of 160 MeV/c is also about 100 ns. The time variations in the trigger can be as large as $\sim$ 50 ns. Thus, to be fully efficient for charged particles and neutrons above 120 MeV/c, we require a dynamic range of at least 150 ns. The TDCs are set to a nominal setting of 50 ps/count, which yields a range of 205 ns.

The Mod 100 version of the 1872A was specified to meet the needs of our system. We briefly discuss these modifications, some of which have now become standard features. Interchannel isolation, namely the dependence of any time measurement on the activity in other channels, was required to be less than one count. The root-mean-square noise on the time measurement of a fixed start-stop sequence was required to be less than one count. A common start signal arriving at least 45 ns (enable time) before the individual stops would yield a valid time measurement. To minimize delays on the board, the common start signals are routed to the backplane on 100-Ω twisted-pair cables, bypassing the standard microstrip delays. Finally, a capacitor that determines the timeout window ($\sim$ 100 ns) beyond the dynamic range, during which time a hit is not sparsified but was assigned a value of 4095, was set to 82 pF.[15] We note that during the experiment, we take all common signals from the backplane.

The performance of the TDC is illustrated by our electronic calibration procedure. We use a CAMAC pulser (Phillips 7210) to trigger and send a start signal to the TDC and a stop signal, which is fanned out to the test inputs of the CAMAC 2313 discriminators which in turn send stop signals to every TDC channel. However, only every fourth channel is pulsed at the same time. The time delay between the start and stop signals is fixed for 50 events, then incremented by 2 ns to take another 50 events. The procedure is repeated until the entire dynamic range of the TDC has been covered. The TDC values are histogramed in Fig. 17a.Each peak corresponds to 50 entries, and the width of each peak, histogramed in Fig. 17b, is about 1.6 channels. Measurements of single channels pulsed individually with a fixed cable delay yielded widths of less than 1 channel [36–38],

[15] The standard value for this capacitor is 180 pF.

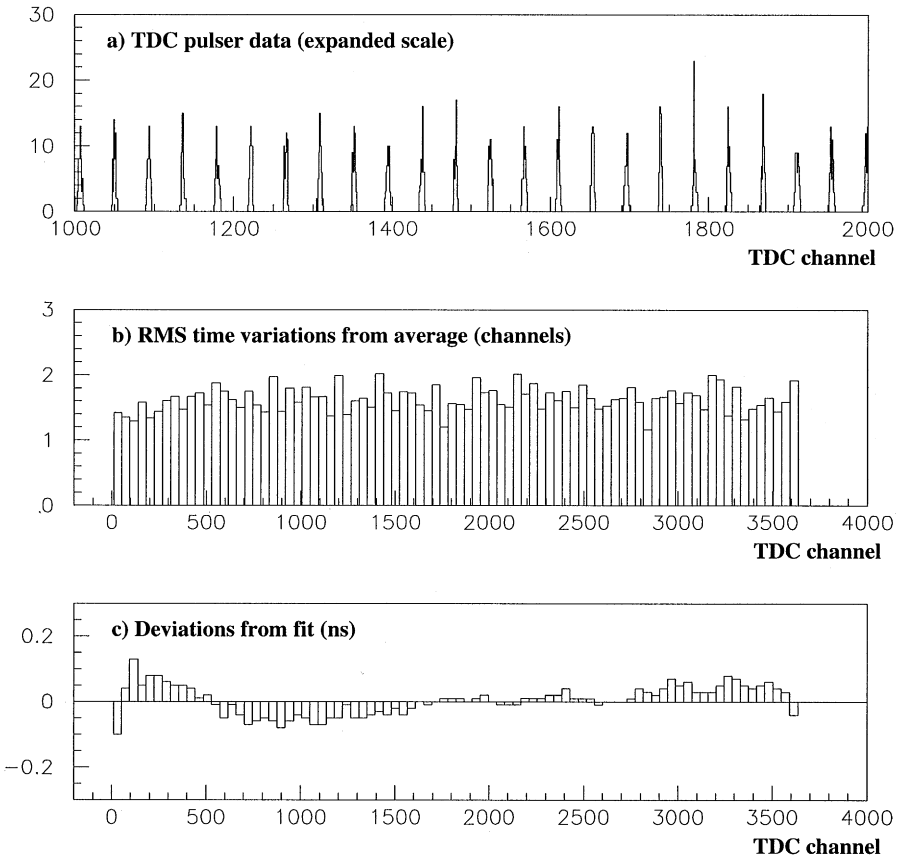

Fig. 17. Sample TDC output. (a) Pulser data taken by delaying the stop signal in 2 ns intervals. The expanded scale limits the display to the middle one-third of the channels analyzed. (b) The rms deviation for measurements taken at a fixed time delay between start and stop signals. (c) The deviation from a quadratic fit to the TDC output as a function of TDC channel. One channel nominally corresponds to 50 ps.

implying the intrinsic width due to the TDC is about 1 channel. The mean values of each peak are then fitted to a quadratic form (see Eq. (8) in Section 4.2.1.2); the deviations are typically 1–2 channels (Fig. 17c).

3.4.5. Analog-to-digital converter

The LeCroy 1881M Analog-to-Digital Converter (ADC) FASTBUS module was selected to record the integrated charge of the pulses from the PMTs. This unit is a 64-channel, 13-bit ADC packaged in a single-width FASTBUS module. It has a fixed conversion time of 12 μs. Input channels with no data are ignored during readout to reduce the data volume and transfer time. The noise, defined as the root-mean-square spread of the pedestal when no input is connected, was measured to be about 50 fC (1 ADC count). The dynamic range is greater than 400 pC [39].

3.4.6. Trigger electronics

To form an efficient trigger, a customized electronics circuit was designed to add the responses from PMTs at both ends to achieve a uniform response across the length of the counter. Since particles can also deposit energy in adjacent counters when they follow a curved trajectory, pulses from adjacent counters must be summed to

obtain an amplitude proportional to the total energy deposited. This summation is performed in the pretrigger circuit shown schematically in Fig. 18.The summed pulse is then discriminated.

This discriminator has two outputs. One output is scaled and used in the CLAS Level 1 Trigger [31] to indicate a hit in the TOF counters. The signal from scintillators 1–16 represents the OR of two adjacent counters and is called a "double"; see Fig. 18. Fine granularity is not required in the trigger at large angles due to the mapping of center-of-mass angles to the laboratory. Thus to reduce the number of input lines to the Level 1 Trigger, "double" pulses are combined for counters 17–48 to produce a "triples" pulse. Since the rates at large angles are lower than at forward angles, the triples pulses can be used without increasing accidental coincidences.

A second discriminator output is "ORed" with outputs from adjacent counters to generate the pulse that enables the fast (low-level) discriminator. The purpose of the "ORed" pulse is to measure timing for both counters in the path of a crossing track. When a track deposits enough energy in one counter to pass the pretrigger threshold but not enough energy in the adjacent counter to pass the threshold, the fast discriminator of the adjacent counter is enabled by the pretrigger signal from the first.

This circuit was tested by observing pulses produced from cosmic rays passing through two adjacent counters. The pulse height for the spectrum from individual counters was about the same while the pulse height for events passing through both counters was lower by about 7%, indicating some loss of light for tracks crossing the counters.

The pulse height of the dynode signals depends on position because (1) light is attenuated in the scintillator and (2) pulses from opposite PMTs arrive at the discriminator at different times. The difference owing to relative timing is corrected by

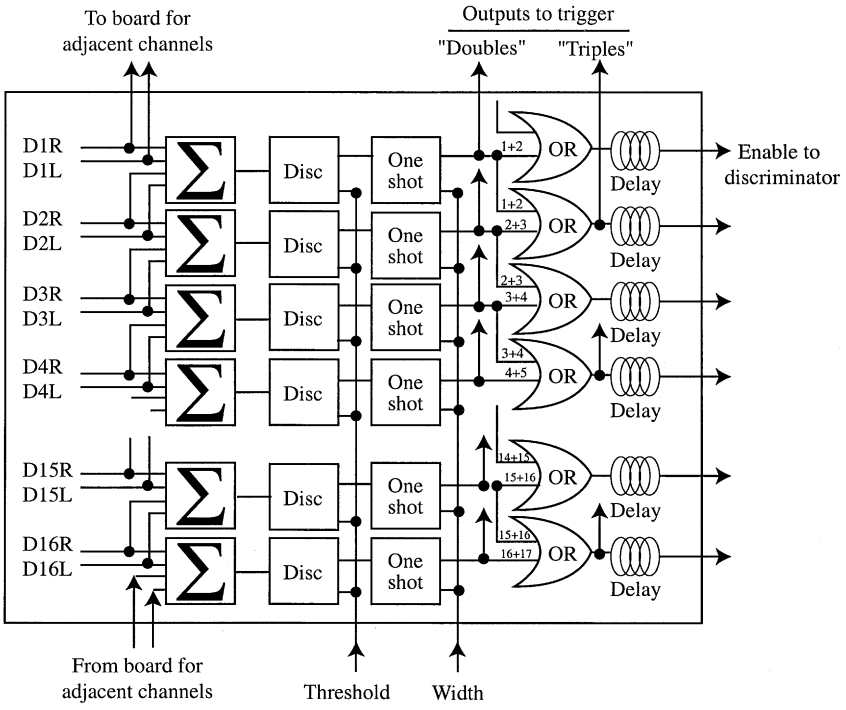

Fig. 18. Logic diagram for the pretrigger circuit. The purpose of the pretrigger circuit is to sum the signals from opposite PMTs to equalize the response along the length of the counter and add the energy deposited in adjacent counters for particle trajectories that cross two counters. The Level 1 Trigger uses doubles from forward angle counters 1–16 and the triples pulses from counters 17–48.

integrating the pulse so as to average the pulse over a time corresponding to the time difference of arrival for tracks at the discriminator. Cosmic-ray tests demonstrated that, as the position of a track moves from an end of the scintillator to the center, the summed pulse height changes by about 20%. When the summed pulse was discriminated, the efficiency was greater than 99% for all positions measured along the scintillators [40].

3.4.7. Pairing of large-angle counters

To simplify the electronics, we paired the last 18 scintillators into nine effective counters with readout at both ends. The PMT signals from the same side of adjacent scintillators were passively summed into a single channel both in the trigger and the readout. The "paired" counters are numbered 40 through 48.

3.5. Start counter

In order to identify particles by TOF, it is necessary to determine the flight time of particles of known momenta through a known trajectory. For experiments with CLAS, the flight time can be obtained by using the electron beam bunch (499 MHz) as the vertex time, and the TOF scintillators to measure the time at the end of the particle trajectory. For experiments with an electron beam, the beam bunch is determined by identifying the final-state electron (with a combination of Cherenkov and calorimeter information), and tracing the $\beta = 1$ particle back to the interaction point. For tagged photon experiments, especially those that have a single charged particle in the final state, independent information about the beam bucket must be obtained from another counter, the Start Counter. The Start Counter is a system of thin counters surrounding the target. Although the design of the CLAS detector initially called for six such counters, practical considerations forced the construction of three coupled counters as described below. These counters have to meet very stringent requirements. They must be thin enough to minimize multiple scattering, large enough to subtend the same solid angle in each sector as the TOF counters, $7^\circ < \theta < 145^\circ$, $-29^\circ < \phi < 29^\circ$, and have sufficiently good time response to clearly identify each beam bucket. The latter requires that the software-corrected time resolution be of the order of $\sigma \sim 350$ ps.

Each counter, covering two sectors, is constructed from a flat sheet of 3-mm-thick BC-408 scintillator. Three such counters form a hexagonal structure surrounding the target. An XP2262 2-in. phototube is attached to the end of each leg to form a double-ended paddle. Attempts to build six double-ended scintillators failed owing to the difficulty of attaching a light guide to the small ("nose") end such that the phototube would not interfere with charged particles produced in the CLAS target or intercept beam halo downstream of the target. Tests with an Ru^{106} beta source show that for charged particles interacting near one phototube, the phototube on the other leg sees approximately 10% of the pulse height of the nearby tube. The time resolution in a test setup ranged from 216 ps (for pulses in the "nose" region which are viewed equally well by both tubes) to 340 ps (for pulses near one tube) with an average of about 280 ps for a uniformly illuminated counter. The times quoted have been corrected for pulse-height slewing. Further details and results are given in Ref. [41].

3.6. Laser calibration system

A system of four ultraviolet (UV) lasers is used to calibrate the TOF counters. The UV light is delivered to the center of each scintillator via a silica optical fiber. The fiber core diameter is 200 μm with a 240 μm cladding. The TDC and ADC information from laser pulses can then be used to calibrate the overall timing and pulse-height time-walk.

The calibration system consists of four optical tables located near the counters. Each optical table contains a Laser Photonics[16] LN203C nitrogen laser operating at 337 nm enclosed in an aluminum box for RF shielding and personnel safety. The laser beam is directed through an opening in the aluminum enclosure to a series of optical and mechanical elements. The laser beam first encounters a flat quartz plate which reflects a small part

[16] Laser Photonics Scientific, 12351 Research Parkway, Orlando, FL 23826.

($\approx$ 4%) of the light back to a fast photodiode[17] circuit which is used as a reference to time the laser to the TOF scintillators. Most of the laser light passes through a variable neutral-density filter[18] with a dynamic range of 1:40. This filter can be used to attenuate the light over a range of values suitable for measuring the time-walk correction of the scintillators. The filter is adjusted by a remotely controlled stepping motor. Downstream of the filter, the beam is expanded by a CTR 5×3 diffuser.[19] The diffused beam incident on the fibers is uniform to within 30%. The beam can then be partially intercepted by a "mask" controlled by a stepping motor. Several different hole patterns along the "mask" can be positioned to illuminate various combinations of fiber bundles. Each bundle consists of seven all-silica 100-μm-diameter fibers (numerical aperture is 0.22) which are 13 m long and distributed to the various scintillators. There are 24 bundle ends which are arranged in a four-by-six rectangular array behind the "mask" within an area of 3.0 cm^2.

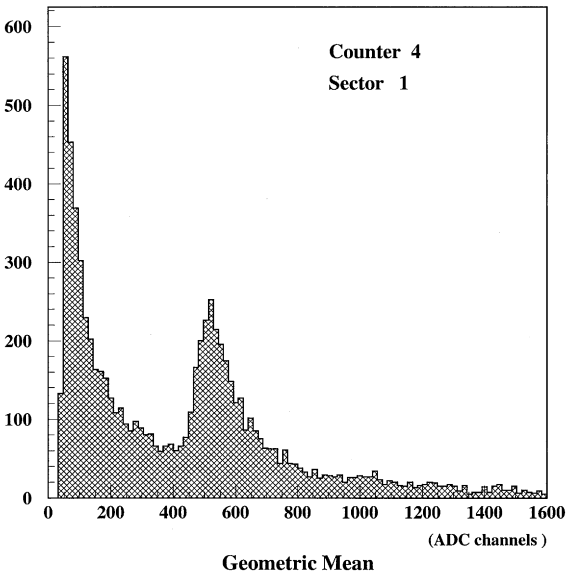

Fig. 19. Typical pulse-height spectrum of all hits in a TOF counter. The energy is estimated by evaluating the geometric mean of right and left PMTs.

4. Performance

4.1. Tests of individual counters

4.1.1. Number of photoelectrons

Two methods were used to determine the number of photoelectrons at the cathode of the PMTs generated by minimum-ionizing particles in the scintillator [10]. The first method divided the pulse height for a minimum-ionizing particle (see Fig. 19) by the pulse height for a single electron. The single photoelectron response from the PMT was measured using an integrating amplifier and an oscilloscope to average the signal. Laser light transmitted to the PMTs was attenuated so that less than one-fifth of the laser pulses, observed by the oscilloscope triggered by the laser, managed to generate a response from the photocathode. The signals measured by the oscilloscope were then assumed to be generated by single photoelectrons. The light intensity was normalized to the intensity of light from a minimum-ionizing particle.

The second method of measurement used statistics to relate the width of the pulse-height distribution to the number of photoelectrons. For this case, the number of photoelectrons is the square of the ratio of the mean pulse height to the standard deviation of the pulse-height distribution. The two methods gave consistent results. The number of photoelectrons generated in the smallest scintillator, 32.3 cm in length, was found to be 1000 ± 100.

4.1.2. Measurement of time resolution with cosmic rays

The timing resolution of the counters was measured with cosmic rays following a method described by Giles et al. [11]. The setup consists of a pair of reference counters A and B above and below the scintillator S under test. All times are measured relative to a common start; then time

[17] P/N Diode, Motorola MRD 500.

[18] Reynard Corporation, 1020 Calle Sombra, San Clemente, CA 92673.

[19] Physical Optics Corp., 20600 Gramercy Pl., Torrance, CA 90501-1821.

differences are used to eliminate timing fluctuations of the start signal. The resolution of the reference system is determined by measuring

$$T_{\mathrm{ref}} = (T_{\mathrm{AL}} + T_{\mathrm{AR}} - T_{\mathrm{BL}} - T_{\mathrm{BR}})/2 \quad (2)$$

in which T_{AL},T_{AR},T_{BL} and T_{BR} are signal arrival times for the PMTs at the ends of the reference counters. The spread in T_{ref}, denoted by σ_{ref}, is equal to the time resolution of each PMT, assuming all four PMTs are equal. Designating the timing for a cosmic-ray particle passing through counter S as

$$T_{\mathrm{S}} = (T_{\mathrm{SL}} + T_{\mathrm{SR}})/2 \quad (3)$$

then the quantity

$$T_{\mathrm{cosmic}} = (T_{\mathrm{AL}} + T_{\mathrm{AR}} + T_{\mathrm{BL}} + T_{\mathrm{BR}})/4 - T_{\mathrm{S}} \quad (4)$$

is the time a cosmic ray passed through scintillator S relative to the reference system. The width of the distribution, σ_{cosmic}, is corrected with the resolution of the reference system, σ_{ref}, to obtain the resolution of S. Thus, with minimum-ionizing particles, the resolution of the TOF counter is the standard deviation

$$\sigma_{\mathrm{S}} = \sqrt{\sigma_{\mathrm{cosmic}}^2 - (\sigma_{\mathrm{ref}}/2)^2}. \quad (5)$$

High voltage on the PMT was set to give a 330 mV signal for a minimum-ionizing particle. The discriminator threshold was set at 20 mV, significantly above the noise level, which was less than 1 mV. The measured resolution for different counter lengths is shown in Fig. 20.

4.1.3. Measurement of time resolution with laser

The time resolution was measured with the laser system with all calibration constants and time-walk corrections included (see below). The laser light is injected into the center of each scintillator and the time recorded in both PMTs. The pulse height was required to be between 300 and 900 channels, corresponding to approximately one MIP. We estimate the time resolution in two ways. First, the average time of both PMTs is computed relative to the measured reference time with the photodiode. Second, we measure the width of one-half the difference of the two signals, which is plotted in Fig. 21 as a function of counter length. This second method

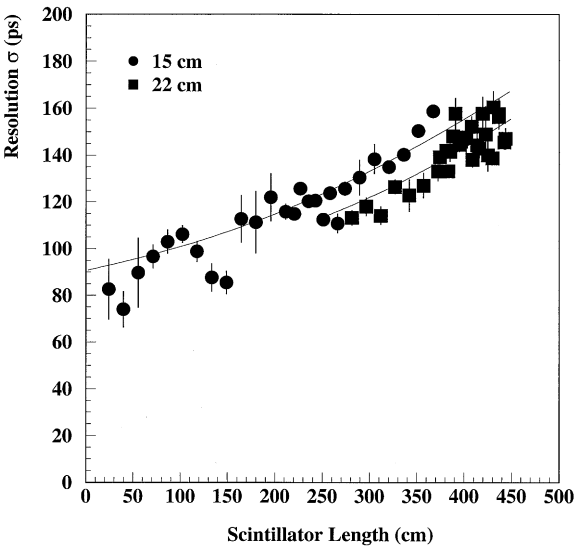

Fig. 20. The timing resolution as determined from cosmic-ray tests for all counters. These measurements were performed on individual counters, providing measurements for 57 counters per sector, before pairing them at large angles. (See Section 3.4.7.) Each data point corresponds to the measured average for six identical counters; the error is the deviation between measurements. The line is a fit to the data using Eq. (6).

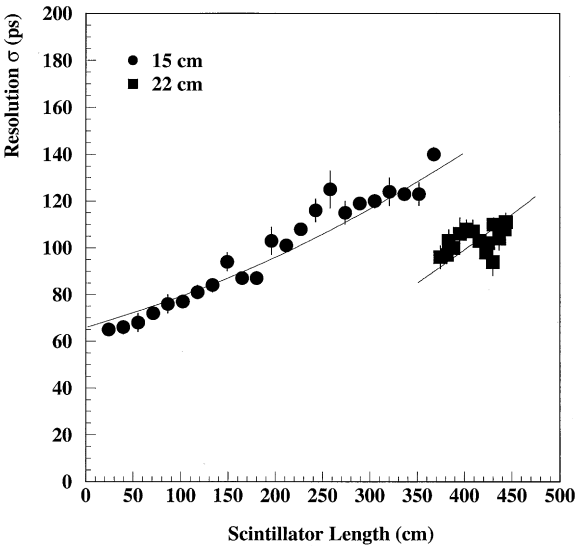

Fig. 21. Time resolution as determined by the laser system for all counters. Each data point corresponds to the measured average for six identical counters; the error is the deviations between measurements. The line is a fit to the data using Eq. (6).

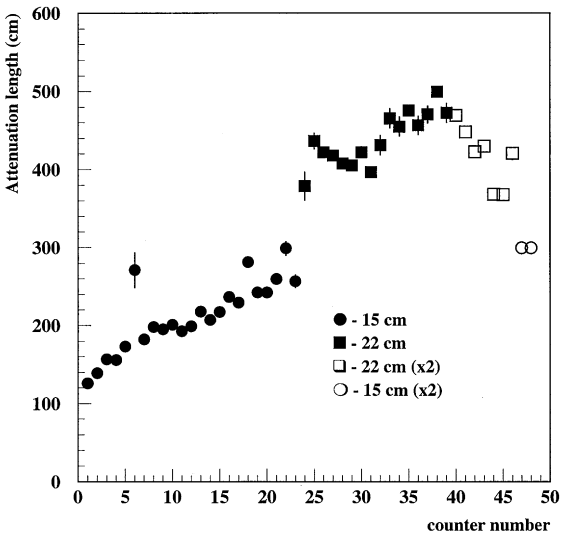

Fig. 22. The attenuation length vs. counter number for all counters.

eliminates all contributions to the timing resolution (~ 100 ps) which are common to both PMTs, including any jitter in the photodiode reference time.

4.1.4. Attenuation lengths and effective velocities

Accelerator beam data were used to extract the effective attenuation length, Fig. 22, and effective velocity for photons, Fig. 23, in each counter. We note that the first two counters are too short to give a reliable measurement of the effective velocity. As the counter length increases, so does the effective velocity because light rays at large angles with longer actual trajectories to the PMT are systematically lost owing to attenuation. These constants are used in TOF analysis to determine the hit position and energy deposition of each event. The intrinsic position resolution is given by $v_{\rm eff} \times \sigma(T^{\rm L} - T^{\rm R})$ for each counter, which is most relevant for the interactions of neutrals. The position for charged particles can be measured more precisely with the drift chambers.

4.1.5. Parameterization of the time resolution

The contributions to the measured time resolution of TOF systems have been simulated in detail [42], and also parameterized as [43]

$$\sigma_{\rm tot} = \sqrt{\sigma_0^2 + \frac{\sigma_{\rm sci}^2 + \sigma_{\rm PMT}^2 + (\sigma_{\rm p} \cdot d)^2}{N_{\rm pe}}} \tag{6}$$

where σ_0 represents the intrinsic resolution of the electronic measuring systems and other processes which are independent of light level, and $\sigma_{\rm sci}, \sigma_{\rm PMT}$ and $\sigma_{\rm p}$ are the single-photoelectron responses for the scintillator, PMT, and path length variations in the light collection, respectively. Path length variations in the scintillator scale with the distance d from the source to the PMT, which we take to be half the length of the counter ($L/2$). The statistical behavior of the last three terms is indicated by scaling the single-photoelectron responses by $\sqrt{N_{\rm pe}}$, where $N_{\rm pe}$ is the average number of photoelectrons seen by the PMT. For scintillators which are several meters in length, the dominant contribution comes from transit time variations of photon paths in the scintillator.

The smooth curves in Fig. 20 represent a fit to the data using Eq. (6). Since the scintillator and PMT response could not be separated in the fit, they were combined

$$\sigma_1^2 = \sigma_{\rm sci}^2 + \sigma_{\rm PMT1}^2$$

$$\sigma_2^2 = \sigma_{\rm sci}^2 + \sigma_{\rm PMT2}^2.$$

The variable σ_1 is the combined single-photoelectron resolution attributed to the PMTs and scintillator on the forward-angle counters, and σ_2 is the resolution due to the PMTs and scintillators on the large-angle counters. The number of photoelectrons $N_{\rm pe}$ in Eq. (6) was calculated, relative to the number $N_{\rm pe}^{\rm o}$ of photoelectrons in the 32-cm long counter, by using the length L and effective attenuation length λ for each counter as follows:

$$N_{\rm pe} = N_{\rm pe}^{\rm o}\, r_{\rm area}\, \eta_{\rm guide}\, {\rm e}^{L_1/2\lambda_1}\, {\rm e}^{-L/2\lambda} \tag{7}$$

where L_1 and λ_1 are the length and effective attenuation length, respectively, of the 32-cm counter. The amount of light reaching the 3-in. tubes is normalized to the 2-in. response by scaling by the ratio of PMT photocathode to cross-sectional area of the scintillator ($r_{\rm area} = 1.29$) and the estimated additional loss of light in the guide ($\eta_{\rm guide} = 0.7$). Both the laser and cosmic-ray data were fit to this form

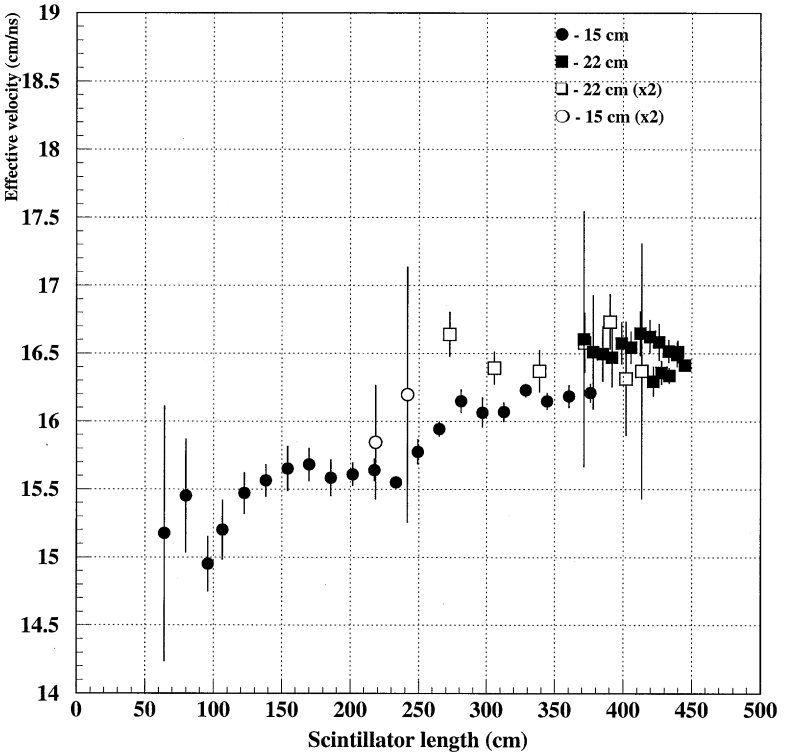

Fig. 23. The effective velocity vs. counter length for all counters. Each data point corresponds to the measured average for six identical counters; the error is the deviations between measurements.

and the parameters obtained from the fit are given in Table 6.

We briefly review the conditions and discuss the measurements for the cosmic-ray and laser data shown in Figs. 20 and 21. The cosmic-ray tests were done on a bench using trigger counters above and below covering a substantial fraction of the counter under test. The measured resolutions were obtained from the average time of both PMTs, which eliminates the position dependence. The contribution of the reference counters was measured and subtracted (see Eq. (5)) to determine the quoted counter resolution. The laser system injects 337 nm UV light into the center of each counter, which is absorbed within a few millimeters of the surface. Since the light originates at a fixed point, we are able to determine the resolution by using the time difference between PMTs. The pulse height was required to be in the range of minimum-ionizing particles.

Table 6
Fitted parameters to the time resolution (Eq. (6))

Parameter	Cosmic rays	Laser
σ_0	62 ± 8 ps	0 ± 1 ps
σ_1	2.1 ± 0.2 ns	2.3 ± 0.1 ns
σ_2	2.0 ± 0.2 ns	0.6 ± 1.0 ns
σ_p	1.18 ± 0.04 ns/m	1.3 ± 0.1 ns/m
N_{pe}^o	918 ± 7	1166 ± 10

This measurement eliminates systematic jitter which is common to both PMTs, and according to the fit, σ_0 is consistent with zero. This constant term is 62 ps for the cosmic-ray data, consistent with our expectations for contributions due to the electronics setup both in the bench setup and also in CLAS. The second parameter (σ_1 or σ_2) includes

statistical contributions from the PMT response, which is the same for both measurements, and the scintillator response. The PMT response terms were obtained under the assumptions discussed in Section 3.2.2.3, yielding $\sigma_{PMT1} \sim 0.55$ ns and $\sigma_{PMT2} \sim 0.34$ ns. There are two differences in the scintillator response between the cosmic-ray and laser data. First, the transit time of cosmics through the scintillator is 170 ps for normal incidence. On the other hand, the laser pulse at the scintillator has a full-width of approximately 800 ps which is deposited at a single point. Second, by not exciting the primary fluor (2.1 ns decay time) the UV light produces a faster rise time (0.9 ns) of the scintillation light. Therefore, we do not expect this term to be identical in the two cases, but similar in magnitude. The fitted parameter σ_1 is the same for both data sets, as expected, and the parameter σ_2 is small for the laser data, but the fitted uncertainty is large. Finally, we note that the width contributions σ_p due to the path length variations are comparable, despite the difference in the position of the light source for the two measurements. This comparison seems to validate the parameterization given in Eq. (6).

4.2. System performance

4.2.1. Calibration

The data for each channel consist of an ADC pulse height A, with a maximum count of 8191, and a TDC time T, with maximum count of 4095. Calibration of the system requires ADC pedestal determination, gain-balancing and gain-matching of the pulse heights, determination of the time-walk correction functions, and relative time offsets of each counter.

Three sources of data were used for calibration: laser light, cosmic rays, and particles created by reactions of 1.6, 2.4, and 4.0 GeV electron beams hitting a liquid hydrogen target. In general, the laser system was used when studying the characteristics of a single counter while times between different scintillators were studied with cosmic rays or beam, as there are large variations in the laser pulse amplitude for different counters and every laser fiber could have a different time offset.

4.2.1.1. Gain-matching. The purpose of gain-matching is to equalize the detector response to crossing tracks. This is a necessary procedure because each counter must contribute equally to the trigger for a common-threshold discriminator level. The gain-matching procedure is accomplished by adjusting PMT high voltages so that normally incident minimum-ionizing particles (MIPs) produce a peak in ADC channel 600 after pedestal subtraction for every counter. The value was chosen from two considerations: the maximum count of the ADC is 8191, and we expect a dynamic range of 8 which sets the upper limit. Also, we want to be above the lowest channels where time-walk corrections are significant. Initial voltages were set using the laser system which matched the gain of PMTs on opposite ends of the same scintillator. The response to particles was accomplished using cosmic-ray muons. Fig. 24, a histogram of the mean value of energy losses by MIPs, shows that the spread of gain matching was about 30% (FWHM), which is adequate for our purpose.

To find the energy deposited, the ADC pulse heights A are first corrected for the ADC pedestal values P; then the pulse heights are scaled to the

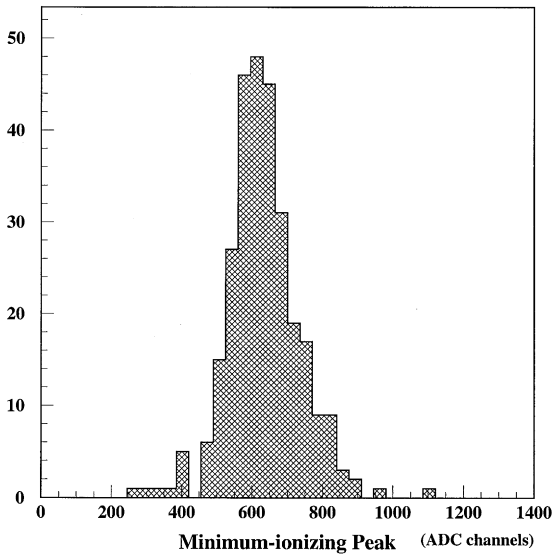

Fig. 24. Results of gain-balancing and matching. The position of the peak of the pulse height for minimum-ionizing particles is plotted for all 288 counters. The desired peak value is 600.

response of normally incident MIPs at the center of the scintillator. The quality of this software energy calibration is indicated by Fig. 25, a scatter plot of energy loss versus particle momentum. The measured pulse height normalized to the calibrated MIP peak value is used to reconstruct the energy deposited in the scintillators. The energy loss of protons increases linearly at low momentum until they begin penetrating the scintillators, at which point the energy loss follows the Bethe–Bloch formula. A weak deuteron band can also be seen in the plot. The pions and protons are clearly distinguished for momenta between 0.3 and 1 GeV/c.

4.2.1.2. TDC calibration. A quadratic equation, which gives a good representation of the data given in Fig. 17, was used to convert the raw TDC data to time units (ns):

$$t = c_0 + c_1 T + c_2 T^2 \tag{8}$$

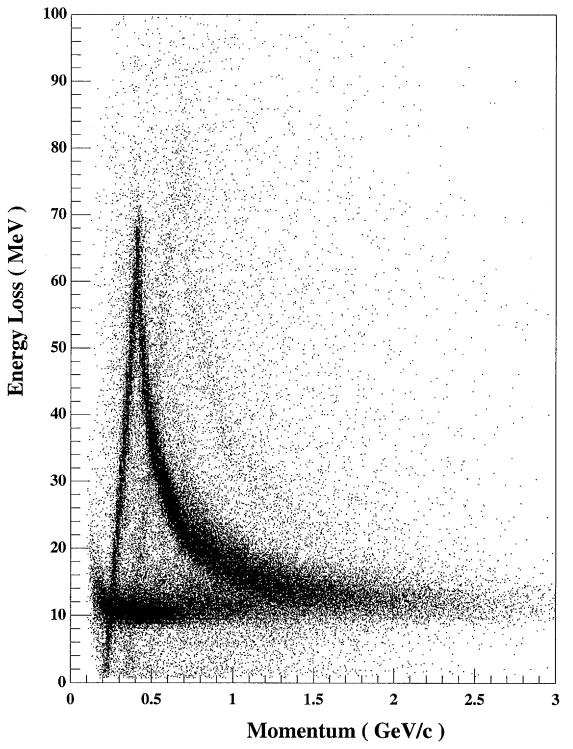

Fig. 25. Energy deposited in scintillator as a function of particle momentum for an empty target. Protons and pions can be distinguished, as well as a faint deuteron band.

where typical values of $c_0 \sim 1$ ns, $c_1 \sim 0.0495$ ns/ch, and $c_2 \sim 5 \times 10^{-8}$ ns/ch^2. The constant terms, arbitrary at this point, were constrained so that the average of the 64 channels of each FASTBUS card was zero.

4.2.1.3. Time-walk corrections. The time-walk corrections, and left–right timing constants, were obtained with the laser system, which delivers a light pulse to the center of each counter. Using a neutral density filter to vary the amount of light delivered to each counter, the pulse height and time were measured for pulses with different amplitudes to obtain the dependence of pulse timing on the pulse height. This dependence is shown in Fig. 26 for a typical scintillator. The measured times correspond to the time of a PMT pulse crossing a fixed (leading-edge) voltage threshold. To correct for time-walk, we perform software corrections of the form

$$t_{\mathrm{w}} = t - f_{\mathrm{w}}\left(\frac{A - P}{V_{\mathrm{T}}}\right) + f_{\mathrm{w}}\left(\frac{600}{V_{\mathrm{T}}}\right) \tag{9}$$

where V_{T} is the channel corresponding to the leading-edge discriminator threshold of 20 mV

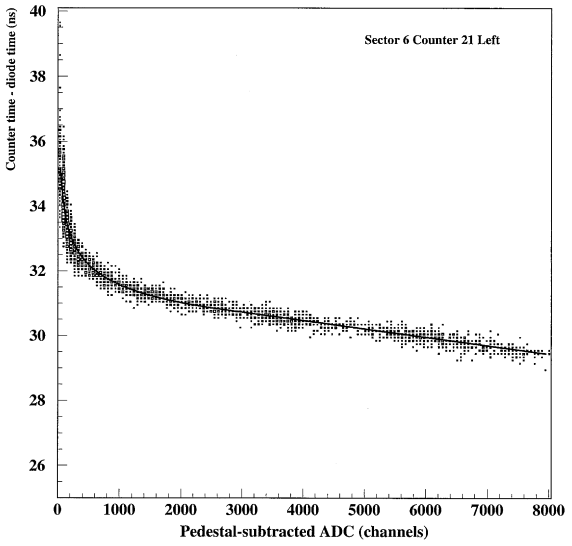

Fig. 26. Typical example of the dependence of the TDC times (ns) vs. the pulse height (ADC counts). The line shows the fitted time-walk function Eq. (10).

(approximately 35 channels), and $f_w(x)$ is the time-walk-correction function described below. This parameterization has the desirable limit that t and t_w are equal for minimum-ionizing pulses in ADC channel 600. The function $f_w(A)$ is a monotonically decreasing function of A since the measured time is late for a pulse with a finite rise time. Our parameterization has three fit parameters w_0, w_2, and w_3. They were determined for each PMT separately using the laser calibration system described in Section 3.6. Fits to data indicate that the time-walk correction is described by a function which first decreases rapidly as a power law, then changes to a slow linear decrease:

$$f_w(x) = \frac{w_2}{x^{w_3}} \quad \text{if } x < w_0$$

$$f_w(x) = \frac{w_2}{w_0^{w_3}}(1 + w_3) - \frac{w_2 w_3}{w_0^{w_3+1}} x \quad \text{if } x > w_0. \qquad (10)$$

The linear part of the curve (ADC $\geq V_T \times w_0$) corresponds to saturation of the PMTs. Monte Carlo calculations demonstrated that the time-walk parameters were not significantly affected by the position of the track through the scintillator [44]. The fitted parameters were obtained for the ADC range between 0 and 8100 counts and typical values are $w_0 \sim 50$ (depends on the PMT), $w_2 \sim 15$ ns and $w_3 \sim 0.07$, with a strong correlation between the last two parameters.

4.2.1.4. Time-delay calibration. The relative time of PMTs on opposite ends of the same counter was determined using the laser system. The reaction $ep \rightarrow e\pi X$ was used to determine the time delays between the 288 counters by comparing the time from a TOF counter to the time of the beam RF [45]. The RF signal from the accelerator has a 2.004 ns period, which is long enough to be resolved by the TOF system by using scattered electrons. The RF bunch length itself corresponds to a few picoseconds, and timing signals are provided by the accelerator as a reference to the experimental areas. Although the timing signals are very accurate, the determination of which bunch produced a given interaction must be made by the experiment. Electrons were identified using information from the CLAS Cherenkov and calorimeter. Pions were selected using energy loss measured in the TOF counters, and momentum and path lengths were calculated using reconstructed tracks in the CLAS drift chambers. The calibration was divided into four steps. First, the difference between the vertex time of pions or electrons, reconstructed from the TOF measurements, and the time of the RF bunch was calculated. This time difference was divided by 2.004 ns and the remainder was taken as the offset correction to the TOF time. However, there remained a 2.004 ns ambiguity since the actual beam bunch, which caused the event, was unknown. In order to correct for this ambiguity, electron–pion coincident events were used. The calibration constants were determined, modulo 2.004 ns, by requiring that the two reconstructed tracks have a common vertex time. In the second step electrons were detected in the first ten forward counters to be calibrated relative to an arbitrary, but fixed, counter with coincident pions. With the forward counters mutually calibrated within each sector, the time delays between the six sectors were aligned using events containing pions in the forward 10 counters of Sector 1 and electrons in the first 10 counters in the five other sectors. In the final step the time offsets for remaining TOF scintillators (11–48 in each sector) were obtained by referencing coincident pions in the counters being calibrated to the first 10 forward counters of all sectors. The result of the calibration procedure is shown in Fig. 27, where the predicted vertex time of electrons in all counters is compared to the RF accelerator time.

4.2.2. Resolution

We can estimate the time resolution of each counter using electron–pion coincidence events. The TOF times are determined by averaging the times of right and left PMTs. The electron track is then reconstructed, and its TOF time is corrected for the flight time back to the target. This time is used to determine which RF bucket contained the incident electron, and we use the accelerator RF time as the true vertex time. The measured vertex time using the pion track is compared to this time to estimate the time resolution of the counter under consideration.

The resolutions for each counter determined in this manner are shown in Fig. 28 as a function of counter length. Scintillators of 100 cm in length, corresponding to a scattering angle of about 18°,

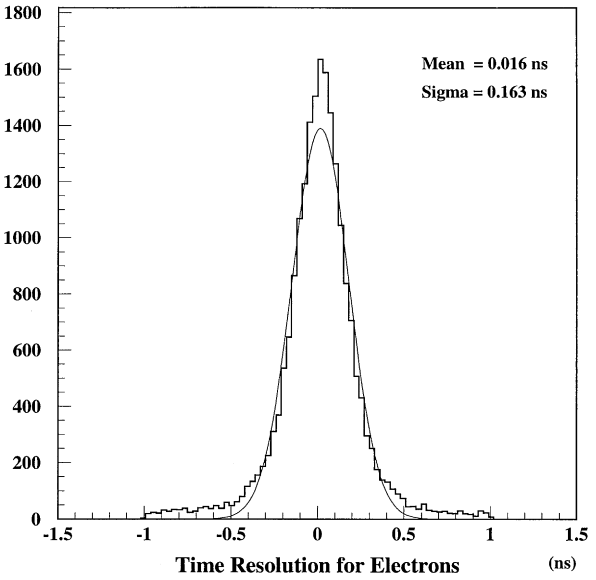

Fig. 27. Time of scattered electrons tracked to the vertex compared to the accelerator RF signal for an incident electron beam of 4 GeV.

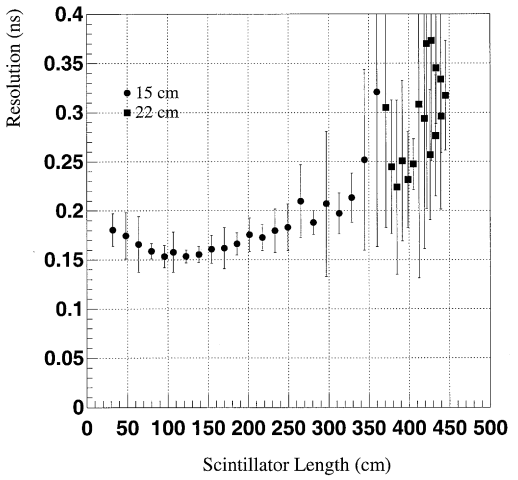

Fig. 28. Time resolution as determined by electron–pion coincidences. Each data point corresponds to the measured average for six identical counters; the error is the deviations between measurements. Paired counters were not yet calibrated and are not included in the plot.

have a measured resolution of 150 ps. At larger angles the resolution slowly degrades as expected as the lengths of the scintillators increase. However, at smaller angles, the resolution also degrades, a result of higher rate or background in these counters. The individual tests reflect the intrinsic resolution of the counters (see Section 4.1.5), but the accuracy in the environment of an electron beam for the first data of CLAS is lower by about 50%. These measurements with beam events include non-optimized time calibration procedures, and momentum and path length contributions from track reconstruction. Nevertheless, the resolution compares favorably with other similar systems listed in Table 1, and the level of particle identification already achieved allows the experimental program in Hall B to reach its goals. As we gain operating experience with CLAS we expect to close the gap between the intrinsic resolution of the system and what is achievable over the course of an experiment.

4.2.3. Particle identification

Particle identification in CLAS relies heavily on the combination of measured charged-particle momenta and the flight time from the target to the respective TOF counters. The vertex time is determined by the accelerator RF, modulo 2.004 ns. The identification of the RF beam bucket with the interaction is accomplished in different ways for electron and photon beam experiments. For electron beam experiments, the beam bucket is identified using the TOF time of the scattered electron, traced back to the interaction point. The TOF resolution of 163 ps (Fig. 27) allows clear selection of the correct beam bucket. For experiments with tagged photons, we use the timing information from the electron detected in thick scintillators in the tagger focal plane [46] to identify the correct beam bucket. The time resolution of 110 ps allows very clean bucket separation. In high-rate experiments, the correct tagger candidate is selected by requiring a tight time coincidence with the Start counter. In both electron and photon runs, the vertex time is thus determined with the precision at which the beam bucket timing is recorded. However, the calibration issues discussed in Section 4.2.1 for the TOF counters affect the quality of the extracted flight time, and thus the determination of the particle masses. In Fig. 29 we

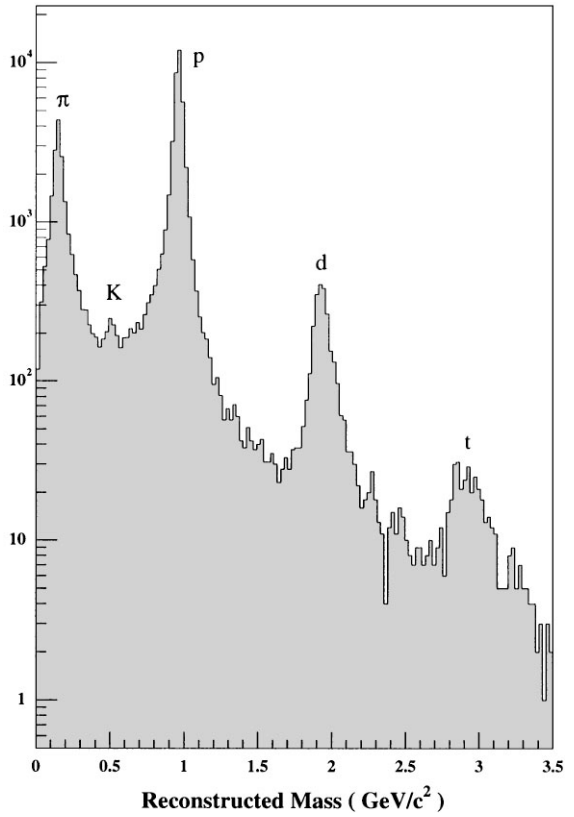

Fig. 29. Reconstructed masses for an empty target run from electrons scattering off the target windows. Clearly visible are the mass peaks corresponding to pions, kaons, protons, deuterons and tritons.

show the distribution of masses for all reconstructed hadrons without any kinematical cuts other than those imposed by the detector acceptance for the February 1998 4 GeV data run. A very clear separation of pions and protons can be seen. A small kaon peak is visible between the two. The mass spectrum also shows nuclear fragments such as deuterons and tritons from the aluminum windows of the liquid hydrogen target.

A plot of velocity versus momentum is shown in Fig. 30, qualitatively displaying the overall particle identification possible with this detector. The sample plotted requires a positive-charged track with a mass between 0.3 and 0.7 GeV^2/c^2 to enhance the kaon signal. The pion and proton bands come from other particles in the same events.

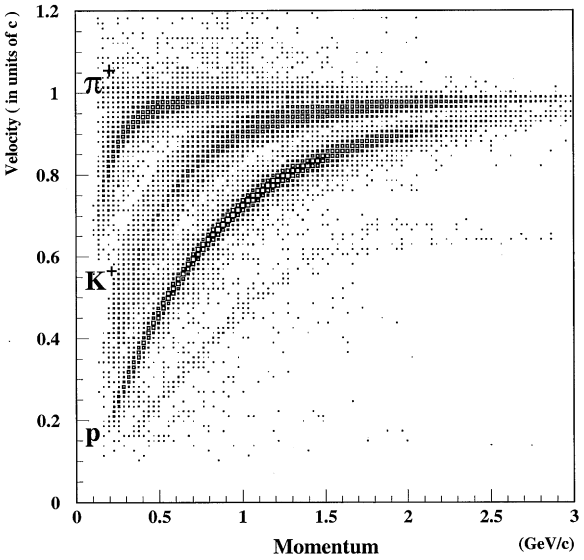

Fig. 30. Velocity of positive hadrons versus momentum. The sample includes a loose selection of kaons, which enhances this particle type relative to the others.

5. Summary

We have designed and built a time-of-flight system for the CLAS detector in Hall B at Jefferson Lab which covers an area of 206 m^2 and achieves an average time resolution for electrons of 163 ps. When combined with magnetic analysis, this detector allows selection of specific particles in the final states of electron and photon interactions. During the first experiments with CLAS, particle identification has been limited by track and momentum reconstruction and the relative calibrations of individual counters.

We have determined the timing resolution of the counters in the CLAS TOF system in three different ways: with cosmic-ray measurements of individual counters in a test setup (Section 4.1.2), with the installed laser calibration system (Section 3.6), and with reconstructed eπ coincident tracks using the first electron beam data in CLAS (Section 4.2.2). These measurements span the range from individual laboratory tests to full-scale implementation of a complex detector. The complement of similar counters of many lengths has allowed us to examine a useful parameterization for the time

resolution of plastic scintillators. The various parameters have been given physical interpretations, so that this parameterization may be used to predict the performance of other counters, or to optimize the time resolution and balance the cost of a new system. The first data with CLAS show that calibration issues in a large system are equal in importance to the intrinsic resolution of individual counters.

Acknowledgements

We gratefully acknowledge the contributions of the Hall B engineers and designers J. O'Meara, W. Tuzel and P. Hemler, and the Jefferson Lab detector group, R. Wojcik, C. Zorn and S. Majewski. We benefited from several discussions with W. Brooks, V. Burkert and D. Doughty, and are grateful to R. Lusk for assistance with the procurement of very specialized items. J. Martz drew many of the figures, S. Corneliussen suggested corrections to several drafts, and the William and Mary Machine Shop under J. Bensel fabricated several special components and assemblies for the system. Finally, a large number of students and technicians assisted in this work over the span of several years: S. Kincaid from Christopher Newport U.; S. Armstrong, H. Faulkner, C. Gliniewicz, A. Penn and T. Petersen from Jefferson Lab; K. Kim, B. Lee, D. Lee and K. Park from Kyungpook National U., S. Korea; G. Briggs, R. Hochreiter and B. St. Hilaire from the U. of New Hampshire; J. Aftosmis, J. Botson, C. Hall, J. Haverlack, S. Kettler, C. Liddle and R. Milner from V.P.I.S.U.; H. Llewellyn from V.S.U.; and W.R. Hall, C.H. Hoff, J.I. McIntyre, M. Mizenko, R. Myers, T. Pavey, J.W. Staren and C.R. Wakefield from William and Mary.

This work was supported in part by DOE Contract #DE-AC05-84ER40150, DOE grant DE-FG02-88ER40410, and NSF grants NSF-PHY-9112528 and NSF-PHY-9207000.

References

[1] F. Binon et al., Nucl. Instr. and Meth. 153 (1978) 409.
[2] W. Braunschweig et al., (DASP Collaboration), Nucl. Instr. and Meth. 134 (1976) 261.
[3] V. Sum et al., (E813 collaboration), Nucl. Instr. and Meth. A326 (1993) 489.
[4] R. Heller et al., (ARGUS collaboration), Nucl. Instr. and Meth. A235 (1985) 26.
[5] Y. Kubota et al., (CLEO II collaboration), Nucl. Instr. and Meth. A320 (1992) 66.
[6] G.C. Bonazzola et al., (OBELIX collaboration), Nucl. Instr. and Meth. A356 (1995) 270.
[7] S. Banerjee et al., (E735 Collaboration), Nucl. Instr. and Meth. A269 (1988) 121.
[8] J.S. Brown et al., (MARK III Collaboration), Nucl. Instr. and Meth. 221 (1984) 503.
[9] J.M. Benlloch et al., (DELPHI collaboration), Nucl. Instr. and Meth. A292 (1990) 319.
[10] J.M. Benlloch et al., Nucl. Instr and Meth. A290 (1990) 327.
[11] R.T. Giles et al., Nucl. Instr. and Meth. A252 (1986) 41.
[12] T. Alexopoulos et al., Phys. Rev. 64 (1990) 991.
[13] G. Sanders et al., Nucl. Instr. and Meth. 180 (1981) 603.
[14] TOPAZ Collaboration, Study of e^+e^- annihilation phenomena by a detector with particle identification, TRISTAN-EXP-002, January 1983.
[15] W.B. Atwood, Time-of-flight measurements, presented at the SLAC Summer Institute, July 28–August 8, 1980. Also SLAC-PUB-2620, October 1980.
[16] E.S. Smith, S. Stepanyan, R. Wojcik, C. Zorn, Light attenuation in large plastic scintillators, CLAS-NOTE-92-007, March 1992.
[17] The initial phase of testing is described by S. Majewski, in Test timing setup for TOF PM's, CEBAF Internal Note, June 12, 1990.
[18] E.S. Smith, R. Jacobs, Photomultiplier tests for the CLAS TOF, CLAS-NOTE-91-003, February 1, 1991.
[19] E.S. Smith, E.L. Faulkner, PMT acceptance tests for the forward-angle CLAS TOF scintillators, CLAS-NOTE-92-017, December 4, 1992.
[20] E.S. Smith, J. Distelbrink, H. Llewellyn, the Detector Group, Tests of 3-inch photomultiplier tubes for the CLAS TOF, CLAS-NOTE-93-015, September 1993.
[21] Ball et al., First tests of a CLAS TOF scintillator at UNH, CEBAF Internal Note, January 1992.
[22] K. MacArthur, J. Distelbrink, CEBAF Large Angle TOF Prototype Photomultiplier Circuits, CLAS-NOTE-94-021, October 1994.
[23] C. Hoff, J.I. McIntyre, E.S. Smith, R. Welsh, R. Winter, Design and testing of light guides for the CLAS detector, CLAS-NOTE-90-016, December 4, 1990.
[24] J.W. Staren, C.H. Hoff, R.E. Welsh, Further studies of light guides for CLAS-TOF scintillators, CLAS-NOTE-91-027, December 31, 1991.
[25] W.R. Hall, R.E. Welsh, T.J. Hallman, Optimized design of low cost light guides for plastic scintillators, CLAS-NOTE-92-019, December 30, 1992.
[26] T. Massam, Nucl. Instr. and Meth. 141 (1977) 251.
[27] R. Winston, J. Opt. Soc. Am. 60 (1970) 245.
[28] K. Wick et al., Nucl. Instr. and Meth. B61 (1991) 472.

[29] E.S. Smith, R. Jacobs, Photomultiplier tests for the CLAS TOF, CLAS-NOTE-91-003, Feb. 1991.
[30] J. Flint, E. Smith, Tests of phillips XP4312B/D1 PMT in magnetic field, CLAS-NOTE-94-008, May 31, 1994.
[31] D.C. Doughty et al., IEEE Trans. Nucl. Sci. 39 (1992) 241.
[32] G. Fidecaro, Nuov. Cimento 15 Series X (Suppl.) (1960) 254.
[33] E.S. Smith, Dispersion in commonly used cables, CEBAF TN-91-022, April 1991.
[34] D. Mack, D. Meekins, private communication.
[35] C. Cuevas, C. Smith, E.S. Smith, First-article testing of LeCroy 2313 discriminator for PMT applications, CLAS-NOTE-95-002, February, 1995.
[36] E.S. Smith, S. Zhou, FASTBUS TDCs for the CLAS TOF, CLAS-NOTE-91-022, October 1991.
[37] T.G. Pavey, E.S. Smith, Tests of pre-production LeCroy 1872A TDC, CLAS-NOTE-93-014, August 1993.
[38] R. Millner, E.S. Smith, Calibrating CLAS FASTBUS TDCs, CLAS-NOTE-93-017, September 1993.
[39] M. Guidal, E.S. Smith, T.Y. Tung, Tests of the LeCroy 1881M ADC for digitization of CLAS PMT pulses, CLAS-NOTE-94-025, December 1994.
[40] D. Jenkins, J. Haverlack, R. Millner, D. Schutt, E.S. Smith, Pretrigger circuit for time-of-flight counters, CLAS-NOTE-94-007, May 1994.
[41] S. Taylor et al., in preparation.
[42] E. Chen et al., Tests of a high resolution time of flight system based on long and narrow scintillator, hep-ex/9606007, August 22, 1998.
[43] M. Kuhlen, M. Moszynski, R. Stroynowski, E. Wicklund, B. Milliken, Nucl. Instr. and Meth. A301 (1991) 223.
[44] J. Aftosmis, J. Ficenec, D. Jenkins, E. Smith, Computer modeling of time-of-flight scintillator pulses, CLAS-NOTE-96-017, August 24, 1996.
[45] L. Elouadrhiri, V. Burkert, S. Stepanyan, H. Egiyan, Charged particle identification in CLAS, CLAS-NOTE-98-004, February 20, 1998.
[46] D.I. Sober et al., The bremsstrahlung tagged photon beam in Hall B at the jefferson Laboratory, Nucl. Instr. and Meth. A (1999) submitted.